Journal of
Materials Chemistry A

ROYAL SOCIETY
OF CHEMISTRY

REVIEW

View Article Online
View Journal | View Issue

Check for updates

Cite this: *J. Mater. Chem. A*, 2024, **12**, 17021

Conjugated microporous polymers: their synthesis and potential applications in flexible electrodes

Dun Zhou,†[a] Kongqing Zhang,†[a] Shuqi Zou,[a] Xiaobai Li*[ab] and Hongwei Ma *[ab]

Conjugated microporous polymers (CMPs) are a unique class of porous materials with π conjugated systems and permanent intrinsic porosity, and have a wide range of applications. With the rapid development of intelligent flexible electronic devices, the application of CMPs as a new electrode material in batteries and supercapacitors has attracted more and more attention due to their high redox activity, good physical and chemical stability, rich porous structure and large surface area. Although CMPs are widely used as electrode materials, they usually exist in an amorphous or semi-crystalline powder state with poor processing properties, thus limiting their application as flexible electrode materials. It is particularly important to develop CMPs as flexible electrode materials. In this paper, first, the synthesis of CMPs is reviewed. Second, the application of CMPs in flexible electronics is emphatically introduced. Finally, the problems and challenges of CMPs in flexible electrode materials are discussed. This review provides a comprehensive understanding of CMPs, which will facilitate the application of CMPs as high-performance flexible electrodes.

Received 29th March 2024
Accepted 3rd June 2024

DOI: 10.1039/d4ta02085e

rsc.li/materials-a

1 Introduction

In response to the imperatives of sustainable societal development, a variety of renewable energy production technologies have been developed in the past few decades. The development of smart flexible electronic devices, including flexible supercapacitors, flexible sensors and new mobile electronic devices,[1–7] is gradually becoming the trend of the future. Intelligent flexible electronic devices require low-cost, well-cycled, high-energy and high-power density energy storage materials as energy storage systems. Therefore, the exploration and development of functional flexible energy storage materials (flexible electrode materials) have emerged as one of the most prominent areas of current research.[8,9] The introduction of organic materials will directly affect the structure and electrochemical properties of the electrodes of electronic devices.[10–12] As a novel material category, flexible porous organic functional materials are regarded as candidates for next-generation electronic devices.[13,14] In comparison with traditional ones, organic porous materials offer the following advantages: (a) they are inexpensive and possess excellent photoelectric properties. (b)

Dun Zhou

Dun Zhou graduated from Northeast Forestry University in 2020 with a master's degree in chemical engineering. He is currently a PhD student in Biology at the College of Chemistry, Chemical Engineering and Resource Utilization, Northeast Forestry University, under the supervision of Professor Hongwei Ma. His main research interest includes the study of conjugated microporous polymers in organic sensors.

Kongqing Zhang

Kongqing Zhang received his bachelor's degree in chemical engineering and process from Harbin University of Science and Technology in 2017. Currently, he is a PhD student at Northeast Forestry University. His research interests include the synthesis and application of biomass organic polymers.

---

[a] College of Chemistry Chemical Engineering and Resource Utilization, Northeast Forestry University, Harbin 150040, P. R. China. E-mail: lixiaobai2008@126.com; mahw@nefu.edu.cn

[b] Center for Innovative Research in Synthetic Chemistry and Resource Utilization, Northeast Forestry University, Harbin 150040, P. R. China

† These authors contributed equally to this work.

These materials demonstrate stable electrochemical properties and offer adjustable band gaps. For instance, the redox potential or theoretical charge storage capacity of the material can be tailored through structural adjustments. (c) When porous organic materials are utilized as organic electrode materials, their large number of micropores provides ample contact points, thus enhancing electron and ion transport between the electrode and the electrolyte.[15–17] (d) Porous organic functional materials are characterized by high specific surface area, cross-linked polymer networks, intrinsic porosity and multiple functionalities with the incorporation of various functional groups.

Conjugated microporous polymers (CMPs) are emerging as a representative class of porous organic materials that allow precise control of pore size, chemical characteristics, and the overall structure. These polymers have a purely covalently bonded π-conjugated backbone and a highly interconnected network structure, with pore diameters typically measuring 2 nm or less.[18–22] CMPs can be constructed in various forms, including 2D[23,24] and 3D[25] networks, dendritic polymers[26,27] and branched polymers.[27] Because of these fascinating properties, CMPs have been developed for a range of corresponding applications, encompassing heterogeneous catalysis,[28–30] gas storage,[31] light-harvesting materials,[32,33] chemical sensing,[34] chemiluminescence,[35] photovoltaic materials[36] and electrode materials.[37,38] Although CMPs are widely used as electrode materials, the insolubility and non-processability of CMPs are recognized as serious bottlenecks which hinder their application as flexible electrode materials. This problem arises from their inherent rigid structure and existence as semi-crystalline powders.[39–41] Much of the prior research on CMPs has concentrated on devising novel constructs and polymerization strategies. These efforts typically involve adjusting the size of the constructs to modulate the specific surface area and pore size distribution of the resulting network, without strict morphological control.[19] However, relatively few methods have been reported for the preparation of CMPs of flexible nanostructures.

In recent years, researchers have provided extensive summaries of the synthesis strategies of CMPs and their diverse ranges of applications, offering valuable insights into enhancing the performance of CMPs. However, there is a paucity of comprehensive and in-depth reviews on the utilization of CMPs as flexible electrodes for electronic devices. Therefore, this review provides a comprehensive summary of the research on CMPs in flexible electronic electrodes. First, we provide a comprehensive introductory overview of the synthesis of CMPs. Subsequently, we provide a comprehensive overview of the potential flexible electronics applications of CMPs. The emphasis is primarily on their utilization as anode materials for batteries, cathode materials for batteries, and electrodes for supercapacitors. Additionally, other applications such as ion exchange membranes and luminescent materials are also discussed. Finally, reasonable conclusions and prospects on CMP research in flexible electrode materials are given, aiming to enhance contributions to this field (Fig. 1).

2 Synthetic reactions and methods of CMPs

The network structure of CMPs can be commonly formed through a chemical reaction involving two or more different monomer molecules or *via* the coupling of a single monomer.[17] As a result, the inherent diversity of monomer molecules and reaction groups leads to an extensive range of network structures and molecular functions for CMPs.[42] Designing an efficient and straightforward synthesis route to precisely control

Shuqi Zou

Shuqi Zou received her bachelor's degree from Gannan Normal University in 2021. She is now a graduate student in the College of Chemistry, Chemical Engineering and Resource Utilization, Northeast Forestry University. Her research interests include nerve agent detection, anti-counterfeiting applications of excitation-dependent molecules, and the synthesis of organic luminescent radicals.

Xiaobai Li

Xiaobai Li is currently an associate professor at Northeast Forestry University. She received her PhD degree in Polymer Chemistry and Physics from Jilin University in 2017. Then, she joined Harbin Institute of Technology as a postdoctoral fellow under the supervision of Professor Yao Li. Her research interests are the design and preparation of electrochromic devices.

Hongwei Ma

Hongwei Ma received his PhD degree from the State Key Laboratory of Supramolecular Structure and Materials of Jilin University in 2017. Now, he is a full professor at Northeast Forestry University. His main research interest is the electrochemical preparation of conjugated porous polymers and their potential applications in organic electronics.

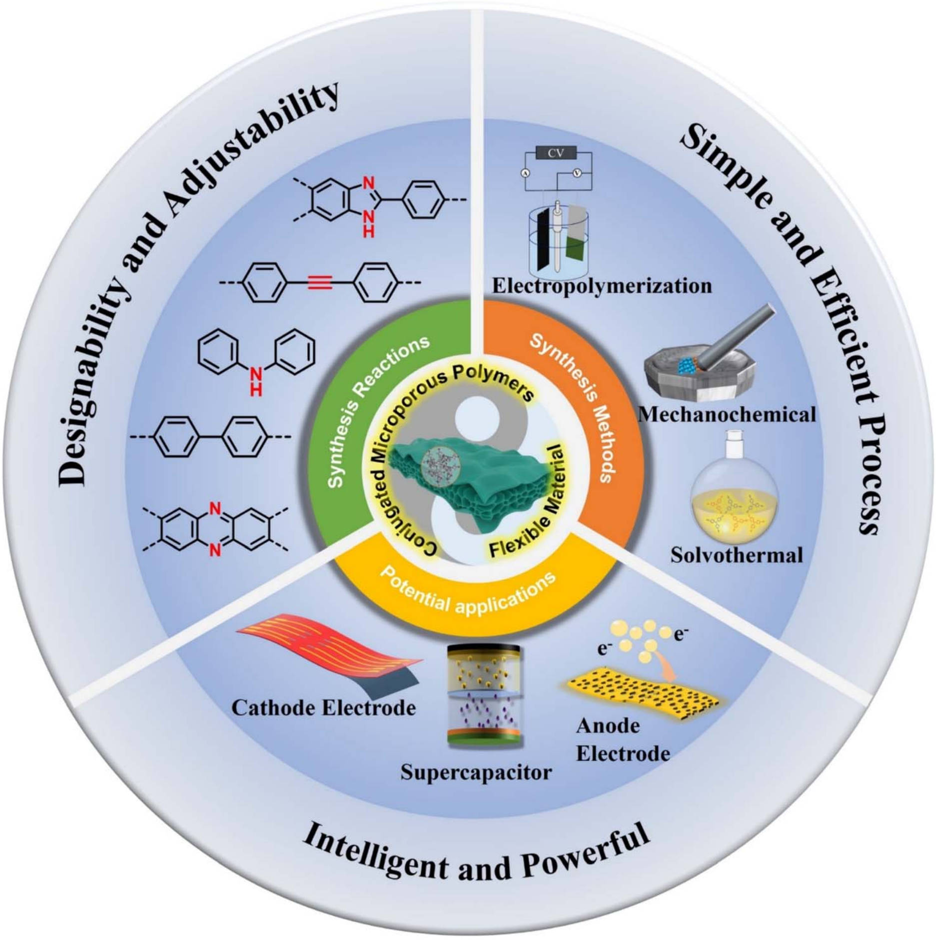

Fig. 1 General content overview: ynthetic reactions and methods for CMPs and application of CMPs in flexible electrodes.

the spatial network structure and photoelectric properties of CMPs involves significant challenges for researchers. Currently, some researchers have overcome this challenge by developing a variety of reaction routes and strategies for the synthesis of CMPs. Using these reaction routes and strategies, researchers can design electrode materials with greater electrical conductivity, larger surface area, and higher electrochemical stability, thereby advancing the development of high-performance energy storage and conversion devices such as batteries, supercapacitors, and electrochemical sensors. This section will delve into the synthesis (including synthetic reactions and methods) of CMPs in detail.

2.1 Synthetic reactions of CMPs

2.1.1 Sonogashira–Hagihara coupling reaction. The formation of conjugated porous structures requires the cross-coupling of modules with varying geometries, and the Sonogashira–Hagihara cross-coupling reaction is a palladium/copper-catalysed cross-coupling of organohalogenated substituents (–F, Cl, Br, and I) with terminal alkyne.[43] The Sonogashira–Hagihara cross-coupling reaction allows the introduction of lightweight alkyne/olefin support units, thereby enabling the formation of conjugated polymers characterized by high specific surface area and stable micropores.[40] In 2014, Jiang *et al.*[44] synthesised a newly designed hexaazatrinaphthalene conjugated microcellular polymer (HATN-CMP) *via* the Sonogashira–Hagihara coupling reaction, which was used as energy storage for lithium-ion batteries (LIBs) (Fig. 2a and b). Compared with monomeric HATN, HATN-CMP showed a capacity of 91 mA h g^{-1} after 50 cycles (Fig. 2c). HATN-CMP retained 62% of its original capacity after 50 cycles (Fig. 2d). In 2022, Mohamed *et al.*[45] reported two pyrene-4,5,9,10-tetrone (PT) linked CMPs (PT-CMPs) as organic electrode precursors for energy storage applications (Fig. 2e). The P-PT-CMP framework demonstrates ultra-high capacitance of up to 400 F g^{-1} (Fig. 2f) with up to 80% capacitance stability after 5000 cycles at 10 A g^{-1} (Fig. 2g). The Sonogashira–Hagihara coupling reaction offers a means to introduce conjugated structures into the polymer backbone, enhancing charge transport capabilities and electrochemical performance.

2.1.2 Suzuki–Miyaura coupling reaction. The Suzuki–Miyaura reaction, in which organoboron reagents are cross-coupled with aryl halogenated hydrocarbons catalyzed by zero-valent palladium complexes, was first reported by Akira Suzuki in 1979.[46,47] With strong substrate adaptability and functional group tolerance, the Suzuki–Miyaura reaction has

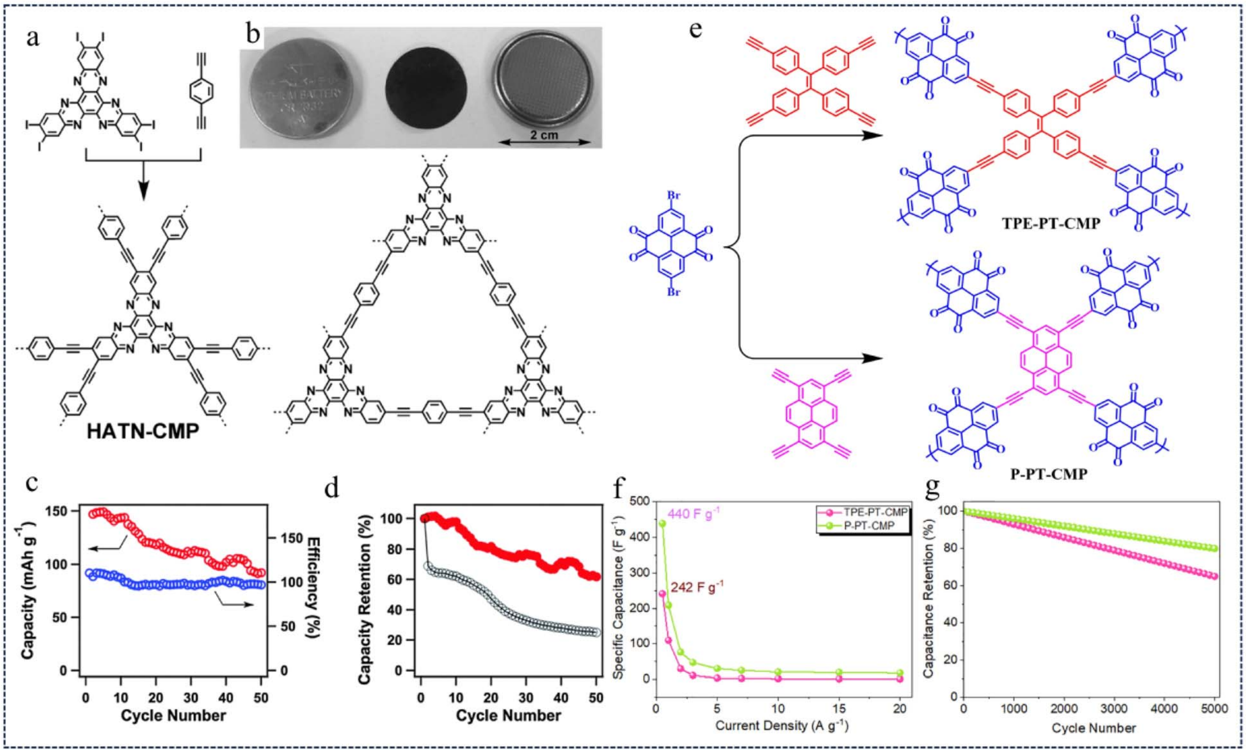

Fig. 2 (a) Synthesis of HATN-CMP networks. (b) The photos of HATN-CMP electrodes. (c) Cycle stability and (d) capacity retention ratio of HATN-CMP.[44] Copyright 2014, Royal Society of Chemistry. (e) Synthetic pathway of TPE-PT-CMP and P-PT-CMP. (f) Capacitance retention and (g) Ragone curve.[45] Copyright 2022, American Chemical Society.

a wide range of applications in organic synthesis. It finds extensive usage in the synthesis of derivatives of polyolefins, styrene and biphenyls, thereby facilitating the synthesis of various natural products and organic materials. In 2016, Cooper *et al.*[48] synthesized a series of CMPs exhibiting various light colors (CP-CMP0, CP-CMP3a-f, CP-CMP4a-f, and CP-CMP5a-f) by incorporating a small number of doped comonomers serving as chromophores within the network. Interestingly, the intrinsic microporosity of these materials led to a notable increase in the absolute fluorescence quantum yield in the solid state (Fig. 3a). In 2019, Xu *et al.*[49] synthesized two series of CMPs by the Suzuki–Miyaura reaction, and employed them as anodes for potassium-ion batteries (KIBs) (Fig. 3b). The polymer PyBT exhibits excellent electrochemical performance and cycling stability for KIBs, with a reversible capacity of up to 428 mA h g^{-1} at 30 mA g^{-1} (Fig. 3c) and a capacity retention of 272 mA h g^{-1} after 500 cycles at 50 mA g^{-1} (Fig. 3d). This work highlights the role of the electronic structure in the rational design of CMP anodes for KIBs with high capacity and long cycle life.

In 2020, Jiang *et al.*[50] prepared a novel CMP, TzThBT, incorporating redox-active substances of triazine (Tz), thiophene (Th) and benzothiadiazole (BT), using Pd-catalyzed Suzuki–Miyaura cross-coupling polycondensation. They discovered its potential as an anode material for LIBs and observed remarkable storage performance for lithium-ions. The polymer anode exhibited a high Li^+ storage capacity of up to 1599 mA h g^{-1} at a current rate of 50 mA g^{-1}. With excellent rate behavior (363 mA h g^{-1} at 5 A g^{-1}) and long-term cycling capability of 326 mA h g^{-1} in more than 1500 cycles at 5 A g^{-1}, this polymer anode offers considerable potential for next-generation LIBs (Fig. 3e). In 2023, Kuo *et al.*[51] prepared a series of CMPs, namely TPP-ThZ, TPP-Th, and TPP-Bz CMPs, characterized by high thermal stability, smooth structure and tunable surface area by using TPP as a constant linker and incorporating three monomers (ThZ, Th, and Bz). It was found that the ability of CMPs for Cr(VI) reduction increased with the increase of thiophene content, owing to different thiophene content, topology and molecular structure (Fig. 3f). Exploiting their redox properties, the development of these CMPs into an electrode for LIBs would result in excellent electrochemical properties.

2.1.3 Heck coupling reaction. First discovered by Richard F. Heck and Tsutomu Mizoroki in the late 1960s, the Heck reaction is one of the most widely used C–C coupling reactions in organic chemistry. This reaction employs a Pd (0) catalyst to couple aryl halides or alkenyl halides with terminal olefins. Notably, the reaction needs to be performed under alkaline conditions and exhibits high regioselectivity and stereospecificity.[52] In 2013, Liang *et al.*[53] constructed a new class of luminescent microporous organic polymers by the Heck coupling reaction of aromatic halides with 1,3,5-tris(4-vinylphenyl) benzene (Fig. 4a). These polymers exhibit notable characteristics including large specific surface area, narrow pore size distribution and strong luminescence performance. As a result,

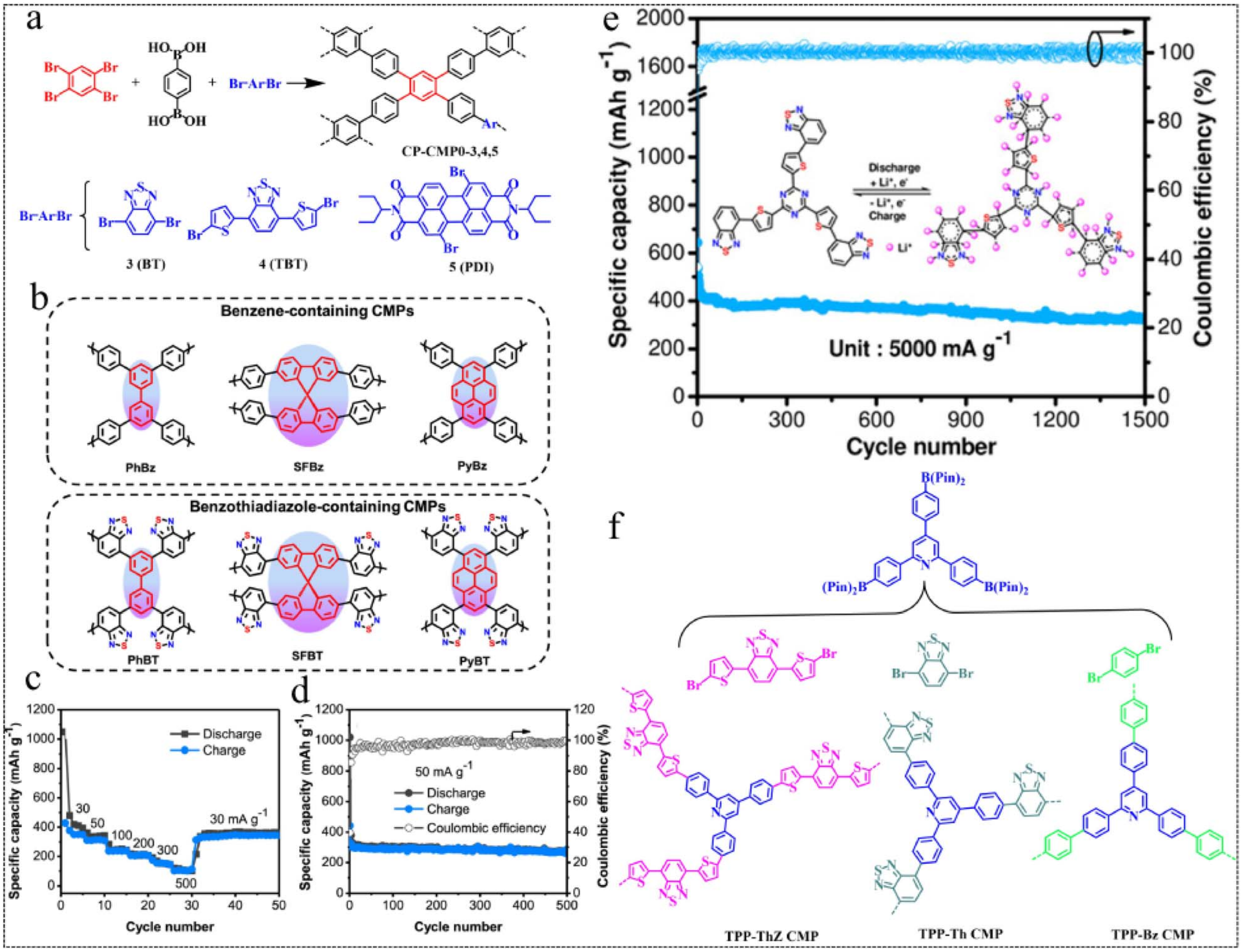

Fig. 3 Suzuki–Miyaura coupling reaction routes. (a) Synthesis of CP-CMP0, 3, 4, 5.[48] Copyright 2016, American Chemical Society. (b) Polymer structures. (c) Rate performance of PyBT. (d) Cycling stability and coulombic efficiency of PyBT.[49] Copyright 2019, American Chemical Society. (e) Electrochemical performance graph of the TzThBT polymer.[50] Copyright 2020, Wiley. (f) Synthesis and chemical structures of the TPP-based CMPs.[51] Copyright 2023, Royal Society of Chemistry.

they hold great promise for various applications in organic photovoltaic cells and photocatalytic fields.

2.1.4 Buchwald–Hartwig coupling reaction. The Buchwald–Hartwig (B–H) coupling reaction, catalyzed by palladium under alkaline conditions, facilitates the formation of C–N bonds between amines and aryl halides, which is crucial for synthesizing aromatic amines.[54] In 2014, Liao *et al.*[55] synthesized a conjugated microporous polytriphenylamine network through B–H coupling, with a Brunauer–Emmett–Teller (BET) surface area of up to 530 $m^2\ g^{-1}$, CO_2 absorption of up to 6.5 wt% at 1 bar and 303 K, along with a selectivity of up to 75% for CO_2–N_2 gas mixtures (Fig. 4b). In 2016, Liao *et al.*[56] synthesised HCMP by B–H cross-coupling using hexa(4-bromophenyl)benzene (HBB) as the nucleus and arylenediamine as the linker (Fig. 4c). HCMP has a moderate surface area of up to 430 $m^2\ g^{-1}$, a narrow pore size distribution, and uniform ultramicropores with sizes less than 1 nm. The porous properties are controlled by the strut length and stiffness of the linker, while the porosity and absorption properties can be modulated by changing the oxidation state of the HCMP. In 2019, Pan *et al.*[57] synthesized four novel luminescent CMPs, LPCMP1-4, characterized by high specific surface area, high chemical stability and thermal stability using B–H crosslinking. They achieved this by modifying the chemical structure of the building blocks, altering the ratio of bromine and amine building blocks, and adjusting the surface area and pore size distribution of polymers through the BXJ (Bristol-Xi'an Jiao tong) method. The studies have shown that LPCMP exhibits highly sensitive and selective fluorescence quenching of nitroaromatic compounds and can be used as a fluorescence sensor for nitroaromatic hydrocarbons (Fig. 4d). Insertion of an arylamine bridge (–NH–) into the CMP skeleton *via* a Heck coupling reaction can improve the discharge capacity of CMP electrodes, resulting in an interesting strategy for high-performance advanced LIB cathode materials.

2.1.5 Yamamoto reaction. Yamamoto coupling, also known as Yamamoto polymerization, is a cross-coupling reaction in which halogenated aromatic hydrocarbons form C–C bonds catalysed by the transition metal Ni.[58,59] In 2010, Cooper *et al.*[60] developed Yamamoto coupling based on tetra(4-

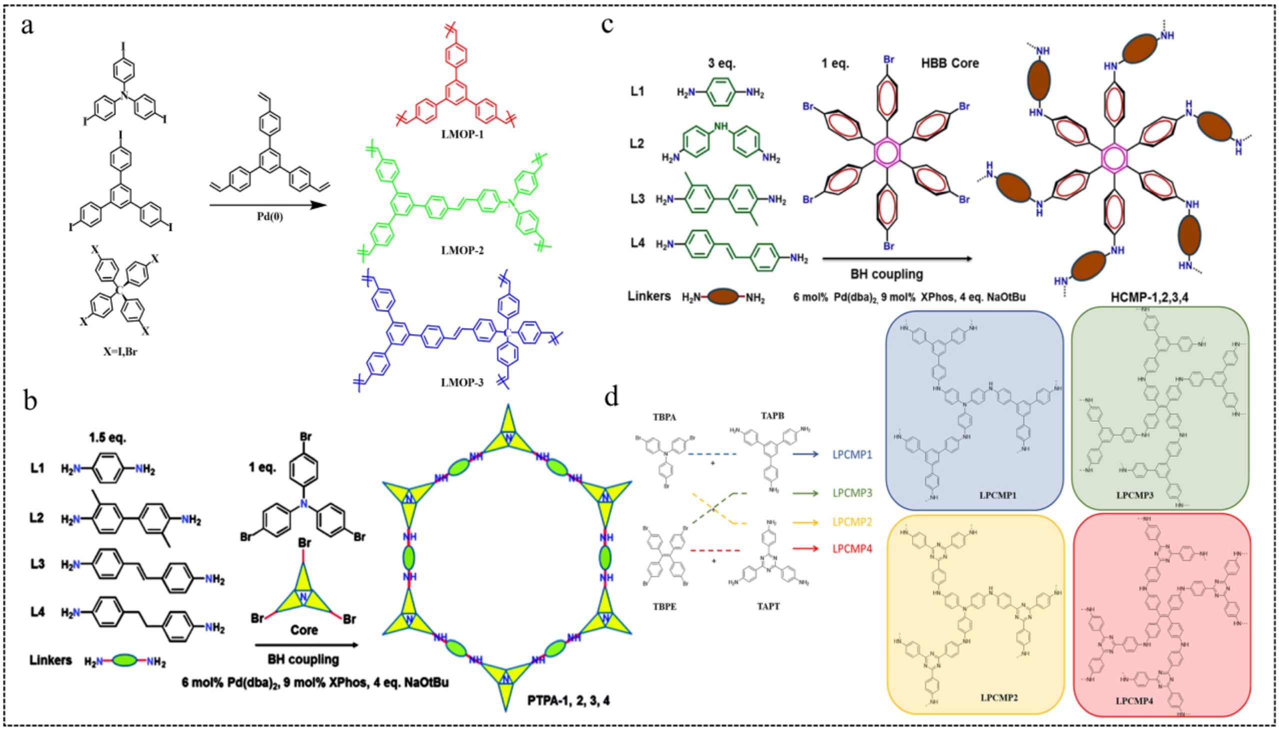

Fig. 4 (a) Syntheses of LMOPs by the Heck reaction.[53] Copyright 2013, Royal Society of Chemistry. (b) Synthetic route to CMP-PTPAs.[55] Copyright 2014, Royal Society of Chemistry. (c) Synthetic route to HCMP-1,2,3,4.[56] Copyright 2016, American Chemical Society. (d) Synthetic route of LPCMP1-4.[57] Copyright 2019, American Chemical Society.

iodophenyl)methane and tetra(4-bromophenyl)-1,3,5,7-adamantane monomers to prepare CMPs of high specific surface area (3160 and 3180 m^2 g^{-1}) (Fig. 5a). In 2009, Thomas *et al.*[61] prepared a series of spirobifluorene-based porous network structures (YSN-CMPs) with high specific surface areas up to 1275 and 1255 m^2 g^{-1} using Yamamoto coupling (Fig. 5b). Their findings indicated significant influences of the bond length and structure of structural elements on the pore structure and BET surface area of CMPs. In 2020, Liu *et al.*[62] designed and synthesized ferrocene-based CMPs (FcCMPs) by Yamamoto coupling using 1,10-dibromoferrocene and 5,10,15,20-tetrakis(4-bromophenyl)porphyrin (FcCMP-1) or tetrakis(*p*-bromophenyl)methane (FcCMP-2) as building blocks (Fig. 5c). Their results demonstrated the exceptionally thermal and physicochemical stability of FcCMPs, with BET surface areas of 638 m^2 g^{-1} and 422 m^2 g^{-1} for FcCMP-1 and FcCMP-2, respectively. Additionally, due to the interaction between the electron-rich conjugated structure of the polymer and the methyl violet of the cationic group, FcCMP exhibits excellent MV adsorption and desorption properties. In 2022, Zhu *et al.*[63] synthesized Pt(II) N-confused porphyrin and Pt(II) porphyrin-based CMPs *via* the Yamamoto coupling reaction (Fig. 5d). They investigated the structure and property differences of Pt–N_3C and Pt–N_4, revealing that CMP-PtNCP and CMP-NCP exhibited enhanced near-infrared light absorption and narrower band gap compared to traditional symmetric porphyrin-based CMPs. Owing to the asymmetric structure of NCP macrocycles, NCP-based CMPs offer new opportunities for further study of asymmetric metal coordination centers for multipurpose catalysis.

2.1.6 Oxidative coupling polymerization. Oxidative coupling polymerization, also known as dehydropolycondensation, refers to the method of oxidative dehydrogenation coupling of compounds containing active hydrogen to form polymers under the action of oxidation catalysts. This process encompasses the polymerization of various compounds such as phenols, acetylenes, aromatic amines, aromatic hydrocarbons, mercaptans and others. Based on different oxidative types, oxidative coupling polymerization is divided into electrochemical oxidation and chemical oxidation. Commonly used chemical oxidants include $FeCl_3$, $AlCl_3$, *etc.*[64–66] In 2018, Chang *et al.*[67] prepared conjugated microporous polybisindolyl maleimide (PBIM) with excellent electrochemical performance as an anode material for LIBs *via* $FeCl_3$ catalyzed oxidative coupling polymerization of bisindole maleimide (Fig. 6a). Due to the reversible cation–π interaction and unique aromatic structure containing N-heteroatoms, the anode material exhibits high capacity (1172 mA h g^{-1}, 50 mA g^{-1}), high cycle life (1000 cycles), and high-rate performance (214 mA h g^{-1}, 2.5C) (Fig. 6b and c). This method offers an efficient strategy and basic platform for the structural design of indole-based CMP anode materials for high-performance LIBs.

2.1.7 Schiff-base reaction. In 2023, Han *et al.*[68] synthesised two imine-linked triazine-based CMPs using a Schiff-base reaction. The CMPs were integrated with carbon nanotubes (CNTs), respectively, using an *in situ*-growth strategy (CNT@TAPT-TPA and CNT@TAPT-BTPA), and then used as anode materials for LIBs (Fig. 6d). Longer cycling stability (specific capacity of 350.9 mA h g^{-1} after 2000 cycles at 1 A g^{-1})

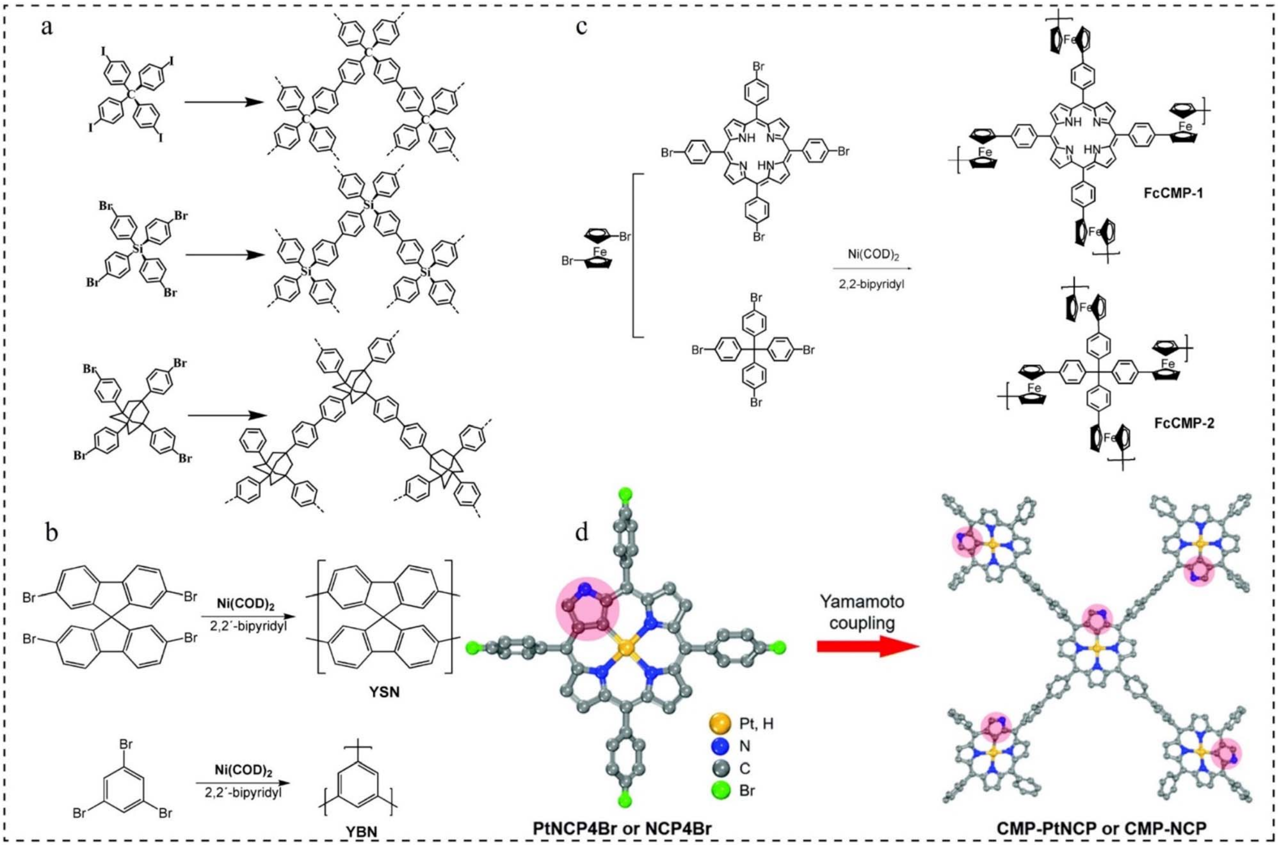

Fig. 5 Yamamoto reaction routes. (a) Synthesis routes to polymer networks 1–3.[60] Copyright 2010, American Chemical Society. (b) Polymerization of YSN and YBN.[61] Copyright 2009, American Chemical Society. (c) Synthesis routes of FcCMP-1 and FcCMP-2.[62] Copyright 2020, MDPI. (d) Preparation of CMP-PtNCP and CMP-NCP.[63] Copyright 2022, Royal Society of Chemistry.

and better rate capability (177.9 mA h g^{-1} at 5 A g^{-1}) were observed for LIBs (Fig. 6e and f). This study provides a rational strategy of molecular design for the development of organic deactivated materials for LIBs.

2.1.8 Heterocycle linkages. In 2021, Wang *et al.*[69] developed visible photoactive triazine-based CMPs (T-CMPs) with high photocatalytic performance and investigated the relationship between their structure and photocatalytic activity (Fig. 7a). Their findings revealed that the photocatalytic performance could be significantly improved by increasing the content of triazine units in CMPs. Specifically, the hydrogen evolution rate of T-CMP-1 (3214.3 μmol h^{-1} g^{-1}) containing more triazine units was much higher than that of T-CMP-2 (242.1 μmol h^{-1} g^{-1}). The results provide a strategy for designing CMPs with high photocatalytic performance suitable for solar-driven hydrogen evolution reactions.

In 2022, Mohamed *et al.*[70] designed a highly efficient and inexpensive, donoracceptor (D–A) system based on CMPs featuring thiazole[5,4-*D*]thiazole (ThTh) linkages (Fig. 7b). This system separates hydrogen from H_2O under visible light without adding any catalyst and uses ascorbic acid (AA) as a sacrificial electron donor. The results show that Py-ThTh-CMP has the highest photocatalytic activity attributed to its high planarity of the Py cell, highly extended conjugation (electron-rich), the strongest absorption in the visible region, narrowest band gap, and strong interaction between the π orbitals of Py (donor) and ThTh (acceptor) units. This results in a hydrogen evolution rate (HER) of 1874 μmol g^{-1} h^{-1}. This study provides a new method for the preparation of efficient photocatalysts and promotes the practical development of efficient hydrogen evolution.

In 2023, Bai *et al.*[71] designed and synthesized two redox-active truxene-based CMPs (Tx-TzTz-CMP-1 and Tx-TzTz-CMP-2) linked by thiazolo[5,4-*d*]thiazole for the photocatalytic reduction of CO_2 to CH_4 (Fig. 7c). The polymer Tx-TzTz-CMP-2, featuring an extended π-conjugated system, exhibited a remarkable CH_4 reduction yield of up to 300.6 μmol g^{-1} h^{-1} and achieved 71.2% selectivity, without the need for any metal cocatalyst and photosensitizer. We note that the use of high-density π-conjugated aromatic heterocyclic linked CMPs for battery electrodes can effectively improve the electrochemical energy storage performance of materials.

2.1.9 Phenazine ring fusion reaction. In 2011, Jiang *et al.*[72] designed and synthesised nitrogen-rich Aza-fused CMPs for supercapacitor energy storage (Fig. 7d). The Aza-CMPs provided a high capacity of 946 F g^{-1}, which was significantly higher than that of other CMPs at that time. A capacity of 378 F g^{-1} was observed at a high current density of 10 A g^{-1} with no decrease in 10 000 cycles (Fig. 7e and f). Based on the results of this

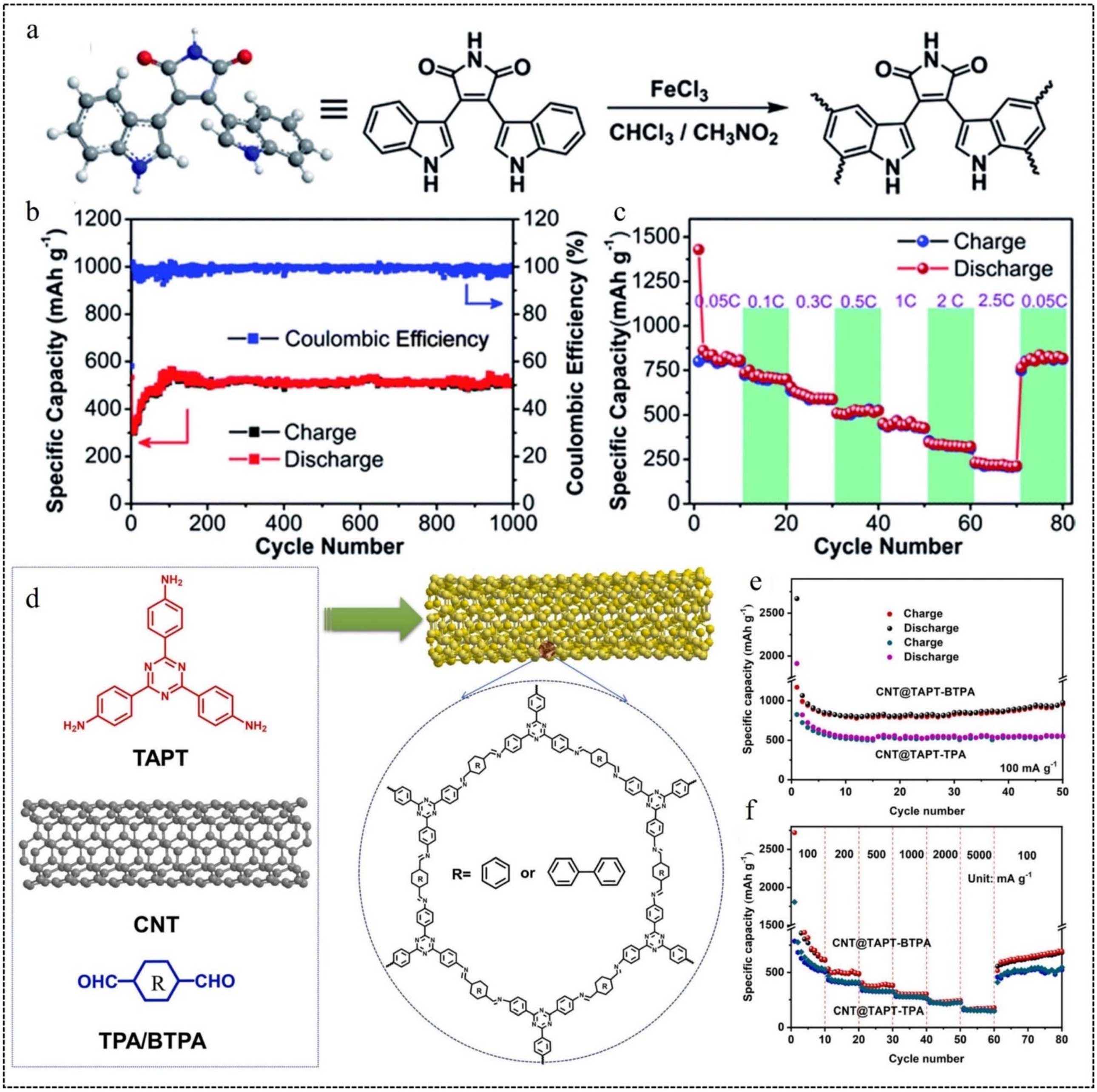

Fig. 6 Oxidative coupling polymerization routes. (a) Synthesis of PBIM. (b) Cycle performance of CMP-PBIM. (c) The rate performance at different current densities from 0.05C to 2.5C.[67] Copyright 2018, Royal Society of Chemistry. Schiff-base reaction routes. (d) Synthetic route of CNT@TAPT-TPA/BTPA. (e) Cycling performance of CNT@TAPT-TPA and CNT@TAPT-BTPA. (f) Rate performance of CNT@TAPT-TPA and CNT@TAPT-BTPA.[68] Copyright 2023, Elsevier.

research, the great potential of *para*-CMPs as high-energy storage devices has been demonstrated.

2.1.10 Cyclotrimerization reaction. Cyclotrimerization usually requires heating of molten salts at temperatures above 300 °C to catalyze polymerization reactions.[73–75] In 2018, Baek *et al.*[75] first reported that phosphorus pentoxide (P_2O_5) catalyzes the direct condensation of aromatic amides to form covalent triazine-based frameworks (CTFs) (Fig. 8a). In the same year, Peng *et al.*[76] exfoliated layered CTF-1 into monolayer and few-layer CTF-1 nanosheets (f-CTF-1) by acid-base intercalation and oxidative exfoliation (Fig. 8b). The high degree of f-CTF-1 stripping significantly improves specific capacitance (about 380% at 1 A g^{-1}) and rate performance when used as a LIB anode. The stripping strategy may open the door to large-scale production of single- or few-layer CTF nanosheets and help to investigate potential applications of CMPs.

2.2 Synthetic methods of CMPs

2.2.1 Electropolymerization method. In the 1970s, electrochemical oxidation polymerization (EP) was proposed and studied by Ambrose, Nelson and colleagues.[77,78] To date, the EP

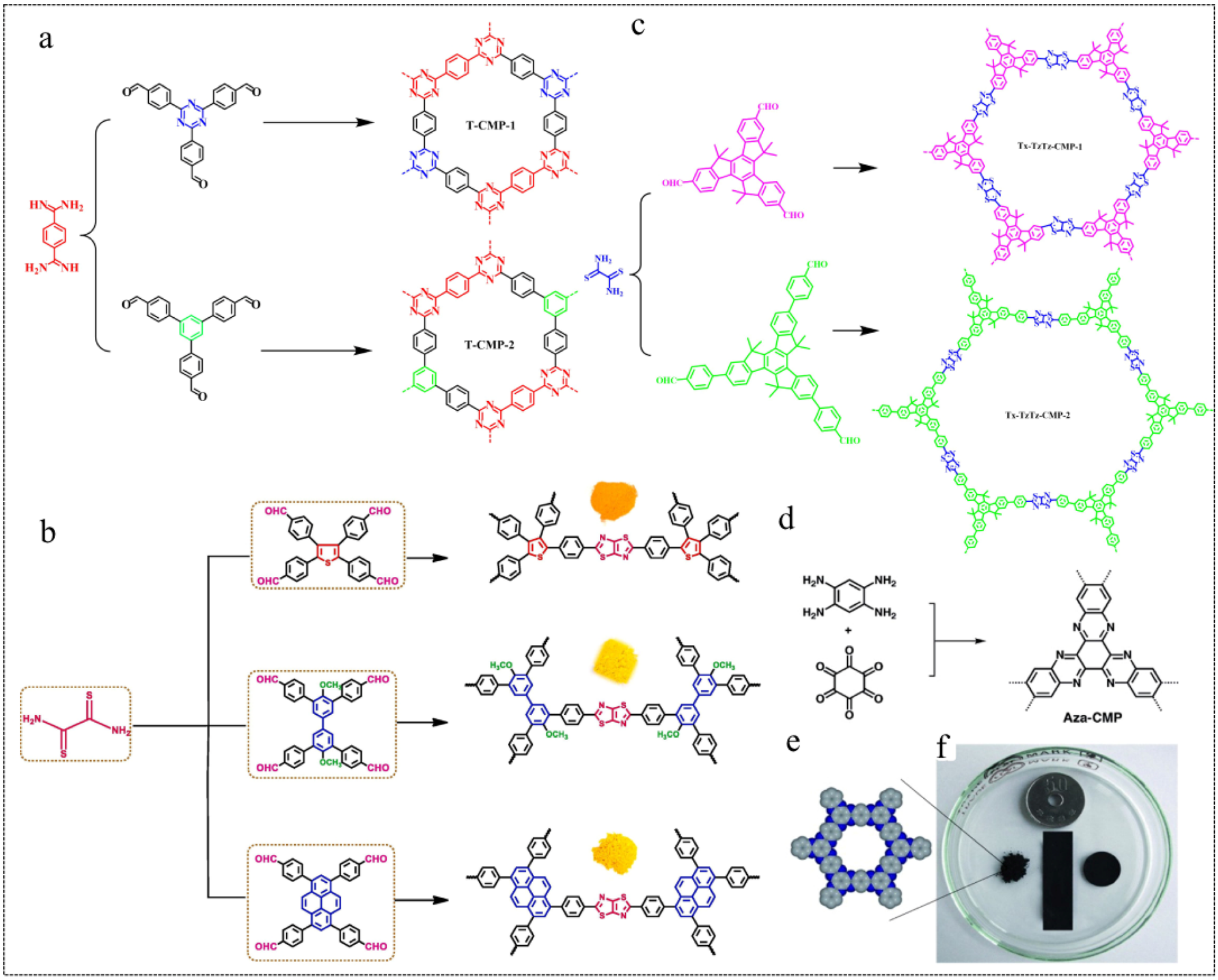

Fig. 7 Heterocycle linkages. (a) Synthesis of T-CMP-1 and TCMP-2.[69] Copyright 2021 American Chemical Society. (b) Synthesis of Ts-ThTh-CMP, Bi-ThTh-CMP, and Py-ThTh-CMP.[70] Copyright 2022, Elsevier. (c) Synthesis of Tx-TzTz-CMP-1 and TxTzTz-CMP-2.[71] Copyright 2023, American Chemical Society. (d) Synthesis of Aza-CMP. (e) The elementary pore structure of Aza-CMP. (f) Photographic image of different shapes of Aza-CMPs.[72] Copyright 2019, Royal Society of Chemistry.

method has facilitated the development of numerous organically constructed units, including thiophene, pyrrole, triphenylamine, and carbazole. The EP method is a widely adopted technique and the most important advantage of EP is that the precursor material can be deposited directly onto the electrode surface under mild conditions without additional catalysts, avoiding secondary processing of the CMPs.

In the EP process, sites with higher electron cloud density in the organic building unit are readily oxidized to form cationic radicals. These cationic radicals exhibit heightened activity, facilitating their interaction with the monomer or other cationic radicals. Furthermore, in the reaction between two cationic radicals, the formation of an ion-pair occurs as the cationic radical bond with the anions in solution. This reduction in electrostatic repulsion promotes the polymerization coupling of the two cationic radicals. Following the coupling reaction, the dimer intermediate undergoes deprotonation and reoxidation to form an aromatic system. Throughout the reaction, a chain-like process persists, involving electron transfer and chemical reaction steps, until the growth of this chain ceases. Furthermore, unlike conventional chemical polymerization, the activity of EP diminishes notably as the reaction progresses, likely attributed to the elongation of polymer chains. Moreover, the deprotonation reaction subsequent to the coupling reaction typically occurs rapidly, propelled by the regeneration of the aromatic system. If the growth rate of the EP membrane is linear, the relative growth rate of the membrane per cycle can be calculated from the following equation:

$$v_{\mathrm{g}} = k\frac{i_{\mathrm{pa}}^{\mathrm{pol}}}{n-1}$$

where "k" is a constant of proportionality. $i_{\mathrm{pa}}^{\mathrm{pol}}$ is the peak current for polymer anodisation, n is the number of cycles ($n \geq 2$), and v_{g} is related to parameters such as cyclic voltammetry scanning speed, concentration of organic building units, *etc.*[79]

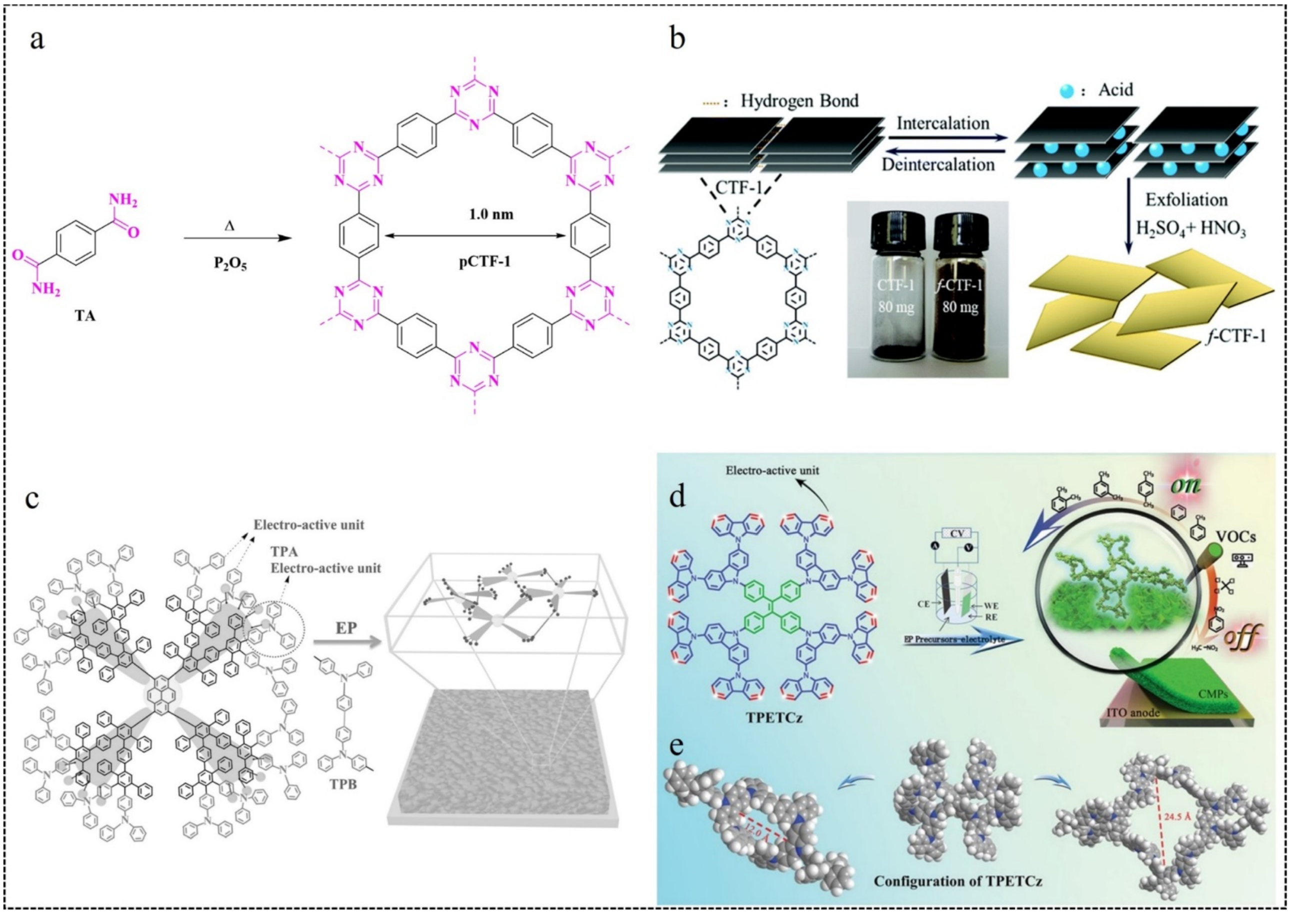

Fig. 8 (a) Synthesis of pCTF-1.[75] Copyright 2018, Wiley. (b) Preparation process of f-CTF-1 nanosheets.[76] Copyright 2019, Royal Society of Chemistry. (c) Dimerisation of TPA with TPB and schematic representation of the crosslinked network microstructure of EP membranes.[80] Copyright 2016, Wiley. (d) EP preparation of TPETCz-CMP films. (e) Structural model of TPETCz-CMP.[26] Copyright 2020, Wiley.

In 2016, we[80] developed the dendritic macromolecule PYT-PAG2 *via* the EP method. We utilized this material as an electroactive precursor to fabricate CMP films with favorable fluorescence properties. By adjusting the EP parameters, they could control the thickness of the fluorescent film and achieve the film as a freestanding membrane on the substrate (Fig. 8c). This study provides a new way to construct fluorescent thin-film sensors from dendrimers.

In 2020, our group[26] employed a straightforward *in situ* electropolymerization method to prepare a film. They utilized a novel dendritic macromolecular material (TPETCz) as the polymerization monomer, notable for its high specific surface area and facilitation of analyte diffusion. The obtained CMP sensor film has a microporous structure with a BET specific surface area as high as 1042.5 $m^2 g^{-1}$. And the selective detection of 18 VOCs was achieved by linear discriminant analysis (LDA) (Fig. 8d and e).

In 2022, our group[81] synthesized two EP films (TCz-CMP and TCzP-CMP) *via* the EP method, employing molecules (TCz and TCzP) with hybridized localized and charge transfer (HLCT) excited state properties as polymerization monomers. In addition, TCzP-CMP had a larger BET surface area (407 $m^2 g^{-1}$) and total pore volume (1.29 $cm^3 g^{-1}$) compared to TCz-CMP, corresponding to pore size distributions of 0.81–1.0 nm and 0.71–0.74 nm, respectively.

2.2.2 Ionothermal method. The ionothermal method represents a straightforward approach for synthesizing CMPs, obviating the need for additional organic solvents to participate in the reaction process.[82] In 2022, EL-Mahdy *et al.*[83] synthesized four pyridine-based CTFs (TPP-CTF) *via* ionic thermal interaction between aromatic nitriles catalyzed by varying molar equivalents of $ZnCl_2$ (Fig. 9a). In 2021, Milner *et al.*[84] realized a new strategy for the solvent-free synthesis of CMPs and PAFs by cyclotrimerization of methyl ketone ions using the aldol reaction (Fig. 9b). These frameworks demonstrated remarkable retention of ultra-high capacitance and exceptional gas adsorption performance, underscoring their potential for large-scale, high-performance supercapacitors, and gas separation materials.

2.2.3 Mechanochemical method. Mechanochemistry can be a solvent-free, timesaving, scalable alternative to the common synthetic routes of porous polymer materials. In 2017, Borchardt *et al.*[85] developed a novel and innovative mechanochemical synthesis method for porous CTFs (Fig. 9c). In 2023, Zhou *et al.*[86] synthesized benzimidazole-bridged conjugated porous polymers (TX-BI-POP) using efficient and

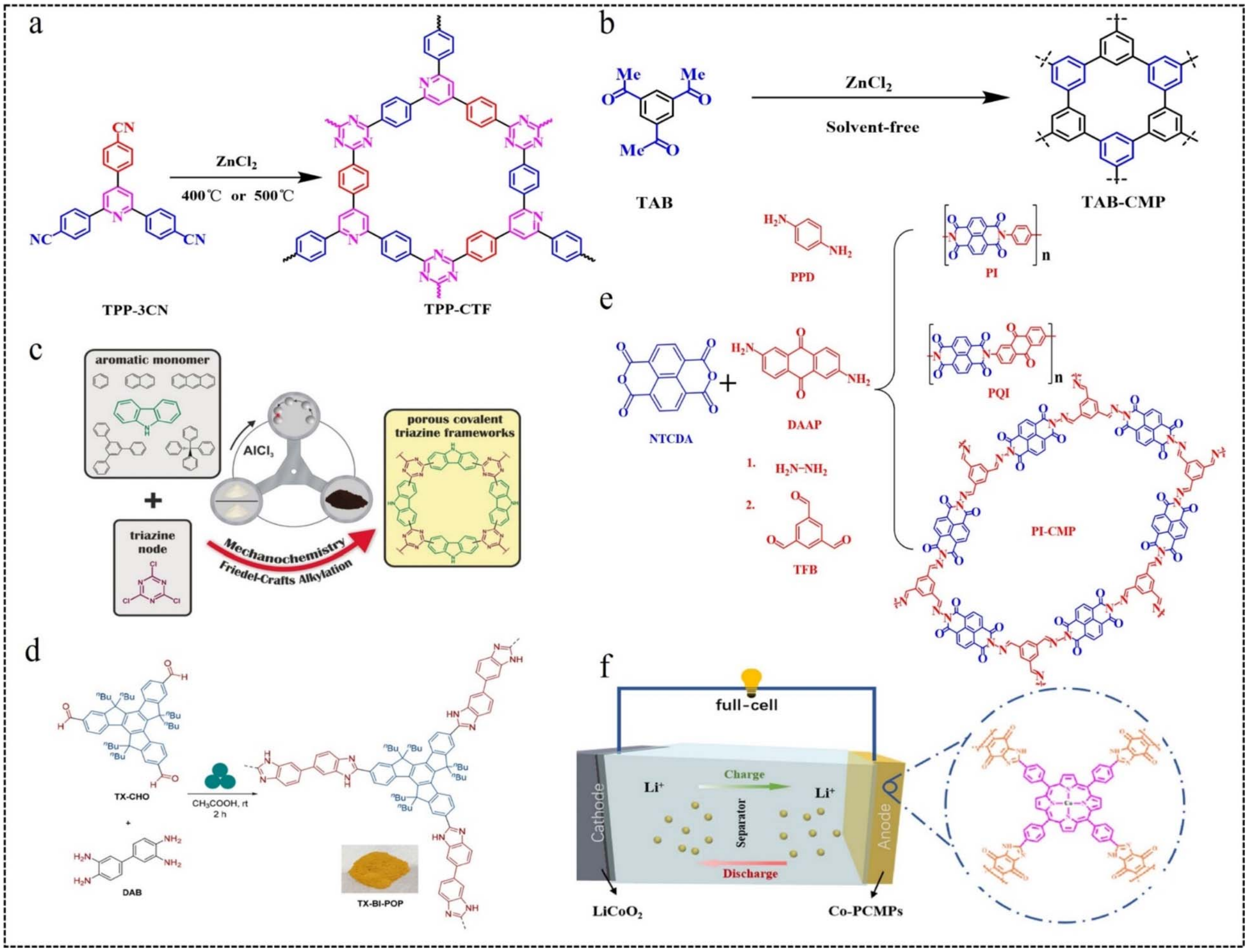

Fig. 9 (a) Synthetic routes of TPP-CTFs.[83] Copyright 2022, Elsevier. (b) Synthesis method of TAB-CMP.[84] Copyright 2021, American Chemical Society. (c) Construction of a porous CTF.[85] Copyright 2017, Wiley. (d) Mechanochemical route to the synthesis of benzimidazole-bridged conjugated porous polymers (TX-BI-POP).[86] Copyright 2023, American Chemical Society. (e) Synthesis routes for 1D PI and PQI polymers and 2D PI-CMP polymers.[87] Copyright 2019, Royal Society of Chemistry. (f) Theoretical cell modelling of Co-PCMPs.[88] Copyright 2022, Elsevier.

environmentally friendly mechanochemical methods (Fig. 9d). They exhibit a variety of photocatalytic activities and redox properties, and can be used as multifunctional photocatalysts and electrodes for LIBs and supercapacitors.

2.2.4 Solvothermal method. Solvothermal methods serve as conventional strategies for CMP synthesis, predominantly involving noble metal synthesis techniques such as the Sonogashira–Hagihara reaction, Suzuki cross-coupling reaction, Buchwald–Hartwig coupling reaction, and Yamamoto reaction, alongside oxidative coupling reactions. These methods offer distinct advantages, including the ability to produce CMPs in large quantities, mild reaction conditions, easy accessibility of substrates, and simpler reaction routes with higher yields, owing to the utilization of a single synthesized precursor. In 2019, Tian *et al.*[87] synthesised a class of organic polymers based on carbonyl groups using a solvothermal method, including two one-dimensional linear polymers, and a two-dimensional conjugated microporous polymer. As a stabilized organic cathode material for KIBs, extended π-conjugation was found to improve cycle stability and rate performance, and the carbonyl group was a potassium ion binding site with excellent reversibility to KIBs (Fig. 9e). In 2022, Cui *et al.*[88] synthesised CMPs (Co-PCMPs) by polycondensation in polyphosphoric acid, which have a porphyrin group with a double active site consisting of a metal-N4 conjugated macrocycle and a conjugated carbonyl group (Fig. 9f). When used as an anode material for LIBs, Co-PCMPs exhibit high capacity (700 mA h g^{-1} at 0.05 A g^{-1}) and excellent multiplicity performance (400 mA h g^{-1} at 1.0 A g^{-1}). The conclusions of this study suggest that the introduction of reactive groups and metal ions greatly improves the capacity of CMPs, which provides more strategies for the further development of organic electrode materials.

3 Potential applications of CMPs

The previous section summarized the synthetic reaction routes and synthetic methods for CMPs, and many researchers have put forward various visions for the preparation of CMPs. Based on these synthetic methods, the chemical structure and macroscopic morphology of CMPs can be largely controlled, and scientific researchers have successively proposed the application concepts of CMPs, which has broadened the application scope of CMPs. In this section, we will mainly summarize the representative applications of CMPs in flexible electrode materials.

3.1 CMPs as anode materials for batteries

Currently, battery anode materials are predominantly categorized into two groups: inorganic and organic materials. When employing inorganic metal materials as anode materials, the formation of dendrites and corrosion on the metal anode is common, resulting in reduced utilization efficiency and poor cycle performance of the metal anodes.[89,90] Organic electrode materials have the advantages of designable structure, low cost and high theoretical capacity,[91–93] but need to overcome the problems of poor conductivity and dissolution in the electrolyte.[94,95]

CMPs have emerged as a novel class of organic electrode materials owing to their high redox activity, exceptional physicochemical stability, highly crosslinked polymer network, abundant porous structure, and expansive surface area.[16,44,96–98] Polythiophene is an n-doped conjugated polymer, but its low redox activity and poor multiplicity performance limit its further development as an anode material for LIBs. In 2018, Xu *et al.*[99] reported a structural design strategy for thiophene-based CMPs with excellent electrochemical performance as anode materials for LIBs. It was found that the thiophene content, crosslinked porous structure, and surface area play a decisive role in improving the electrochemical performance. The poly(3,3-dithiophene) (P33DT) all-thiophene-based polymer has a crosslinked structure and a high surface area of 696 m^2 g^{-1}, whereas polythiophene (PT) has 13 m^2 g^{-1} (Fig. 10a). The pore size distribution (PSD) of the polymers was determined using nonlocal density-functional theory (NL-DFT). P33DT displayed a median micropore diameter of 0.92 nm, while linear PT predominantly showcased graded mesopores spanning from 2 to 20 nm (Fig. 10b). The P33DT exhibits a discharge capacity of up to 1215 mA h g^{-1} at 45 mA g^{-1}, excellent multiplicative capacity, and excellent cycling stability, with a capacity retention of 663 mA h g^{-1} at 500 mA g^{-1} after 1000 cycles, which is 79.9% of the initial reversible capacity (Fig. 10c and d). This work mainly reveals the structure–performance relationship, which further provides a basis for the rational design of CMP anode materials for high-performance LIBs.

In 2020, Zhang *et al.*[98] reported a class of azo-fused CMPs with unique electronic structures as anode materials for rechargeable LIBs. The effect of electronic structure on the redox activity of azo-thickened CMPs was further investigated,

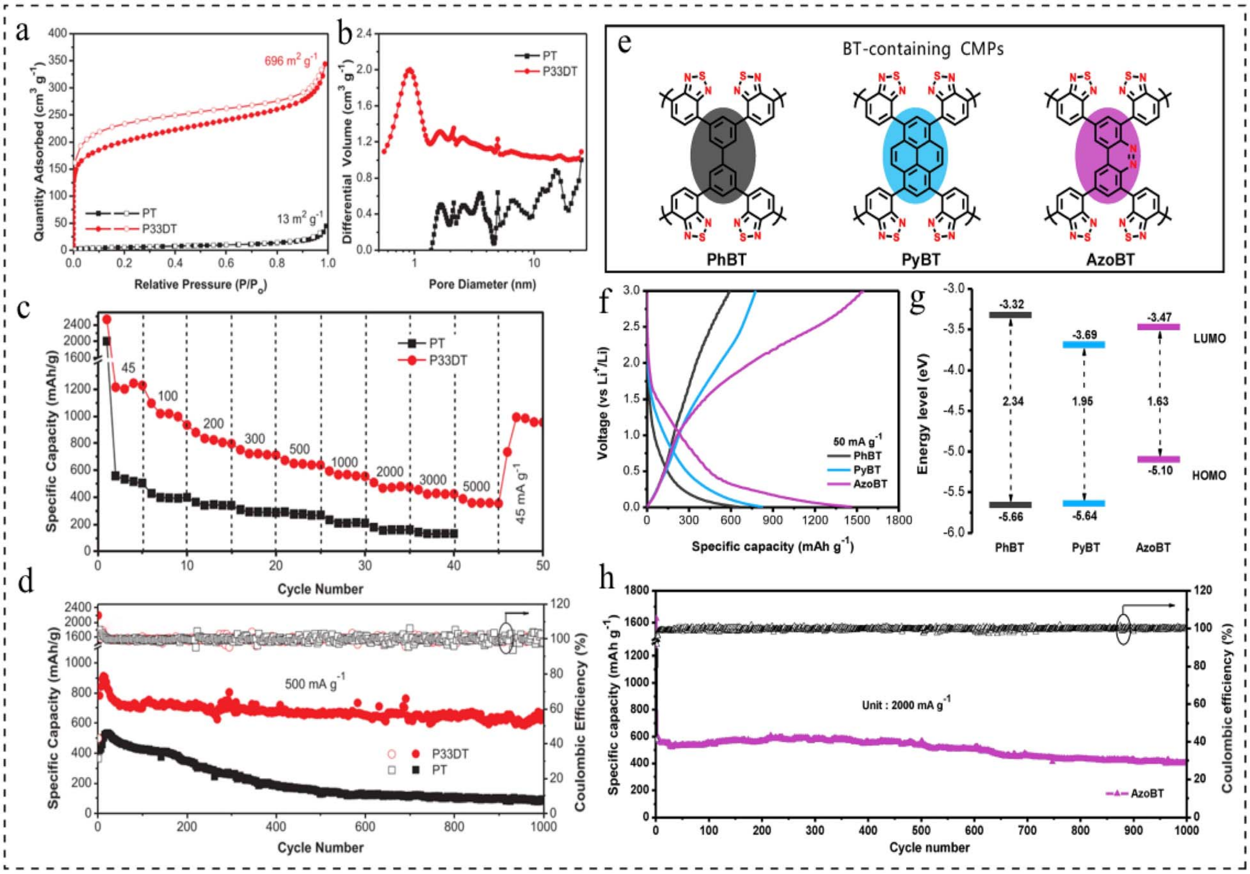

Fig. 10 (a) Nitrogen adsorption–desorption isotherms. (b) PSD calculated by NL-DFT for PT and P33DT. (c) The rate performance at different current densities from 45 to 5000 mA g^{-1}. (d) The cyclability at 500 mA g^{-1} of PT and P33DT.[99] Copyright 2017, Wilye. (e) Conceptual polymer structure of BT-containing CMPs. (f) GCD curves of PhBT, PyBT and AzoBT at 50 mA g^{-1}. (g) The energy level band gap for CMPs containing BT. (h) Cycling stability and coulombic efficiency of AzoBT at 2000 mA g^{-1}.[98] Copyright 2020, Elsevier.

and three materials containing benzothiadiazole (BT) groups (PhBT, PyBT, and AzoBT) were prepared separately (Fig. 10e). The galvanostatic charge–discharge (GCD) testing of the three materials revealed that AzoBT obtained a higher reversible capacity (1534 mA h g^{-1}), followed by PyBT (776 mA h g^{-1}), and PhBT the lowest (591 mA h g^{-1}) (Fig. 10f). Theoretical calculations show that the energy levels of AzoBT, PyBT and PhBT are reduced by 2.34 ev, 1.95 ev and 1.63 ev, respectively (Fig. 10g). The above results demonstrate the significant influence of the electronic structure on the Li ion storage capacity of these CMP electrodes, and that the band gap plays a more important role than the LUMO energy level in the redox activity of the resulting CMPs. In conclusion, AzoBT exhibits higher redox activity due to the presence of N=N redox active centres, which in turn provides more redox activation sites for Li ion storage. The resulting LIBs exhibited ultra-high reversible capacity, excellent multiplicity performance and stable cycling performance (1000 cycles at 2 A g^{-1}) (Fig. 10h).

In 2021, Yu *et al.*[100] developed a new redox donor–acceptor CMP (AQ-CMP) utilizing anthraquinone and benzene as linkers *via* C–C bonding and used AQ-CMP as an ultra-long-life anode for rechargeable air batteries (RABs) (Fig. 11a). AQ-CMP features an interconnected octapole network, which facilitates a favorable electronic structure for enhanced electron transfer efficiency and N-doping activity. Additionally, it boasts a high density of active sites, maximizing the redox capacity based on the weight of the formulation. The AQ-CMP anode yielded near theoretical capacity (202 mA h g^{-1} at 2 A g^{-1}) (Fig. 11b), with excellent multiplicative performance (58% capacity retention at 20 A g^{-1}), and excellent cycling stability (more than 60 000 cycles at 20 A g^{-1}), which was far superior to that of its linear counterpart (AQ-Lin, 73% retention after 250 cycles) (Fig. 11c–g). When combining an AQ-CMP anode with a commercial Pt/C@Ir/C catalyst-based cathode, the resulting CMP air cell demonstrates a consistent specific capacity of 181 mA h g^{-1} at 3 A g^{-1}. Notably, full capacity recovery is solely achieved by refreshing the cathode. Furthermore, by decoupling the electrolyte and cathode design, both the output voltage and voltage efficiency can be enhanced to −1 V and 87.5%, respectively, surpassing those of existing polymer air batteries (Fig. 11h). This research not only enriches the family of redox CMPs and broadens their applications but also offers novel insights into the design of CMP-based electrodes for diverse energy storage systems and other applications.

Porphyrin-based molecules have large π-conjugated aromatic structures, active sites of multi-electron redox activity, and narrow HOMO–LUMO gaps, and are often used as anodes for LIBs.[101,102] In 2022, Zhai *et al.*[103] prepared porphyrin CMPs by Sonogashira–Hagihara cross-coupling of Br-functionalized porphyrin monomers and alkyne-based monomers (Fig. 12a). The CMPs exhibit a notable surface area of 419 m^2 g^{-1} (Fig. 12b) and a narrow bandgap, with optical and calculated values of 1.31 eV and 0.73 eV, respectively. The valence band (VB) spectrum indicates a VB energy (EVB) of 3.81 eV (Fig. 12c–e). Additionally, it achieves a high specific capacity of 1200 mA h g^{-1} at 1 A g^{-1} and maintains a capacity retention rate of 242% after 5000 cycles at 3 A g^{-1} (Fig. 12f and g). These findings present an effective approach for designing and fabricating organic electrode materials characterized by high specific capacity and long-term cycle life.

Alkaline rechargeable batteries (ARBs) are an attractive solution for large-scale electrochemical energy storage applications. However, their development has been greatly hindered by the lack of high-performance and sustainable anodes capable of stable operation with low corrosivity and low electrolyte concentration. However, redox-active CMPs with their robust and mechanically stable 3D microporous structure can provide even better long-life ARBs.[104] In 2022, Patil *et al.*[105] developed high-performance ARBs with anthraquinone-based CMPs (IEP-11)/single-walled CNTs as the anode and commercial $Ni(OH)_2$ as the cathode (Fig. 13a and c). In 1 M KOH electrolyte, when IEP-11 served as the anode, a comprehensive comparison with PAQS showed that IEP-11 had a high specific surface area and total pore volume (738 m^2 g^{-1} and 0.7 cm^3 g^{-1}) (Fig. 13b), high cell voltage (0.98 V) (Fig. 13d), long cycle life (up to 22 730 cycles/960 h, 75% capacity at 20C) (Fig. 13e and f), high specific capacity (150 mA h g^{-1} at 1C) (Fig. 13g), excellent rate performance (90 mA h g^{-1} at 50C) (Fig. 13h) and low-temperature operability (Fig. 13i). The ideas presented in this research not only pave the way for the design of high-performance and advanced ARBs, but also the possibility of developing safe, environmentally friendly and practical organic batteries by utilizing nickel-based cathodes and less corrosive aqueous electrolytes.

3.2 CMPs as cathode materials for batteries

CMP materials have some unique properties due to their large π-electron conjugated structure: (1) good electron transport properties, (2) most CMP materials are structurally stable and rigid, making them difficult to dissolve in conventional electrolytes, and (3) large specific surface area and microporous structure. These properties make CMPs a good choice for building battery cathode materials.

In recent years, some researchers have discovered that conductive polymers with good electronic conductivity and rich redox functional groups are promising candidates for the construction of high-energy aqueous zinc batteries. In 2021, Liu *et al.*[106] prepared a multi-hollow poly(triphenylamine)-CMPs cathode material (m-PTPA) *via* a solvothermal synthesis strategy (Fig. 14). The cathode material has a more regular porous structure similar to the covalent organic frameworks (COF) material, facilitating the accommodation of Cl^- in a pseudocapacitive-dominated manner for energy storage purposes. Moreover, its specific 3D organic framework-shaped conjugated porous network can significantly increase the N activity (up to 83.2% at 0.5 A g^{-1}) and stability (87.6% capacity retention after 1000 cycles) of the material. This electrode material also enabled the zinc ion battery device to have a high energy density of 236 W h kg^{-1} and a maximum power density of 6.8 kw kg^{-1}, which is a significant advantage over organic zinc ion batteries reported at the same time. This study provides new ideas for the rational design of CMP organic cathode materials.

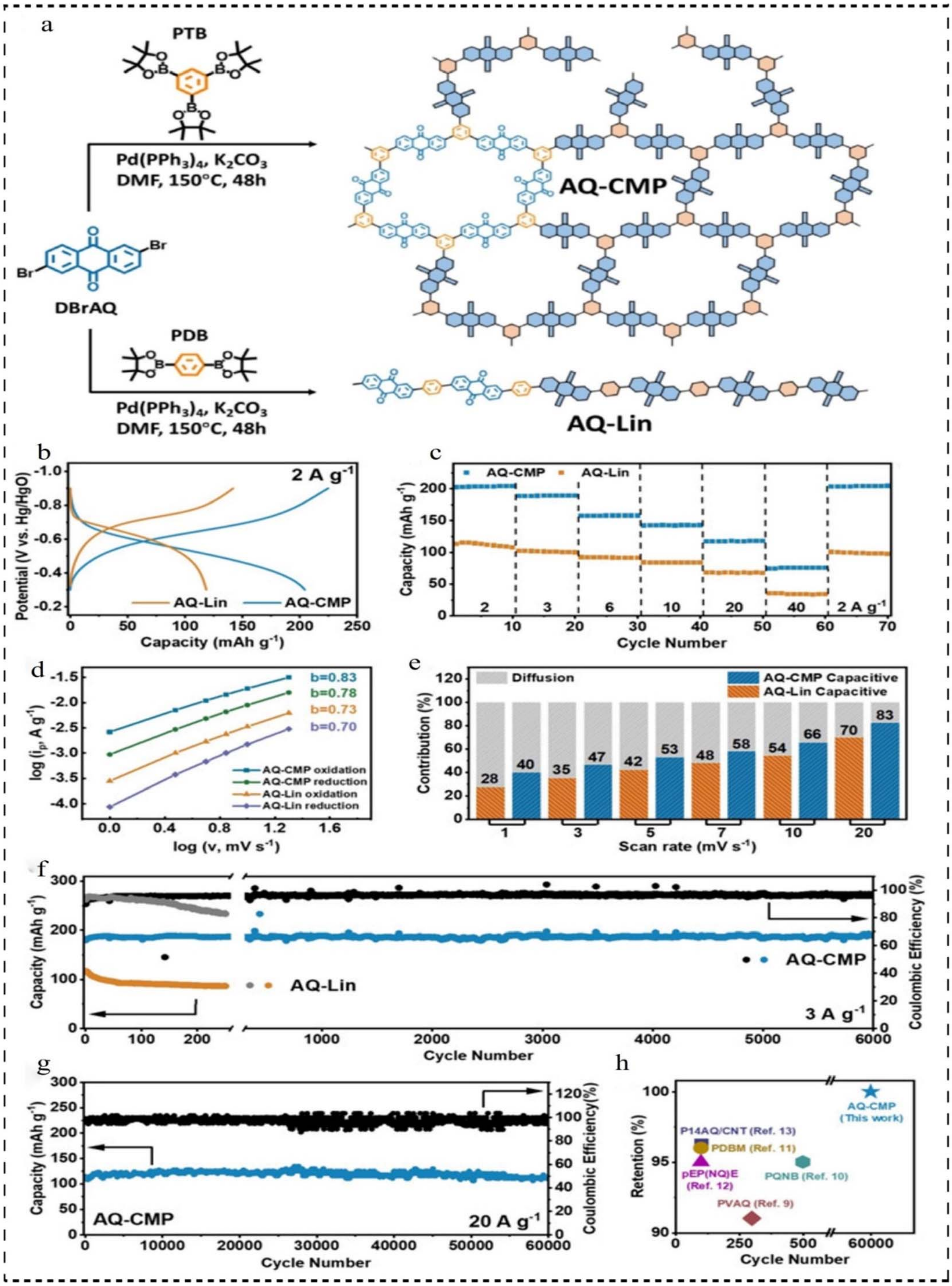

Fig. 11 (a) Synthetic route of AQ-CMP and AQ-Lin. (b) Comparison between AQ-CMP and AQ-Lin based on GCD curves at 2 A g^{-1}. (c) Rate capability at different current densities. (d) *b*-value analysis. (e) Normalized percentage capacitive contribution at different scan rates. (f) The long-term GCD stability tests of AQ-CMP and AQ-Lin at 3 A g^{-1}. (g) The long-term GCD stability tests of AQ-CMP and AQ-Lin at 20 A g^{-1}. (h) Capacity retention comparison of various polymer anodes for RABs.[100] Copyright 2021, Wiley.

Rechargeable aluminum batteries (RABs) use redox active polymers as cathodes to address the problems of slow inorganic cathode kinetics, low capacity, and poor integrity.[94] Recent studies have found that n-type phenozines have high capacity, reversibility and rapid redox kinetics in aqueous electrolytes due to the presence of C═N double bonds. In 2023, Bitenc *et al.*[107] reported for the first time a phenazine-based hybrid microporous polymer (IEP-27-SR) for use in an organic cathode in aluminum batteries with $AlCl_3$-EMIMCl ionic liquid electrolytes (Fig. 15a and b). The cyclic voltammetry (CV) curve of the Al//IEP-27-SR cell shows two pairs of reversible redox peaks at about 1.1 V (peak O1 and R1) and about 0.6 V (peak O2 and R2),

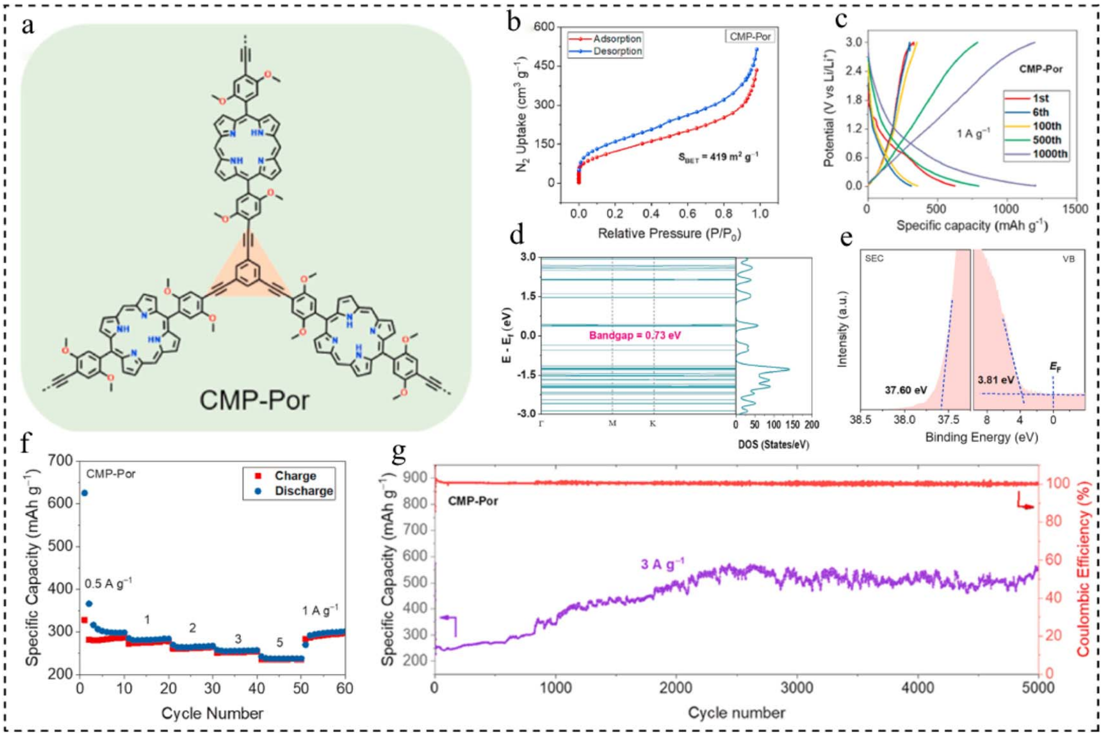

Fig. 12 (a) Structure of CMP-Por. (b) BET test for CMP-Por. (c) GCD profiles at 1 A g^{-1}. (d) Density of states of CMP-Por. (e) Ultraviolet photoelectron spectroscopy of CMP-Por. (f) Rate capability. (g) Long-term cycle life at 3 A g^{-1}.[103] Copyright 2022, Elsevier.

which are believed to be due to the reversible reduction/oxidation of the phenazine portion of the polymer structure (Fig. 15c). The electrochemical performance of the Al//IEP-27-SR battery was evaluated by GCD at different C-rates, and the specific capacity decreased as the current density gradually increased (Fig. 15d). At a minimum current density of 0.5C, the highest specific capacity value of 116 mA h g^{-1} was obtained, with a high coulombic efficiency (CE) of 99% (Fig. 15e). By evaluating the cycle life of the battery, in the first 250 cycles, the battery showed a capacity retention rate of 99% and a capacity of 98 mA h g^{-1}. 75% of the initial capacity was maintained after 3440 charge–discharge cycles (127 days of continuous cycling) at 1C (Fig. 15f and g). This study improves battery performance and paves the way for the development of advanced multivalent batteries by providing an efficient pathway for the movement of ions and electrons.

In the construction of dual-ion batteries (DIBs) with redox-active building block polymer cathodes, p-type dihydrophenazine (Pz) unit modules have attracted extensive attention due to their high reversible redox reaction and high theoretical charge storage capacity.[108–111] However, most of the reported Pz-based polymer cathodes still have problems such as low redox activity, slow kinetics and short cycle life. To address these issues, in 2021, Zhang *et al.*[112] developed a CMP (TzPz) cathode material based on donor–acceptor (D–A) dihydrophenazine, by assembling the electron-donating Pz unit and the electron-withdrawing 2,4,6-triphenyl-1,3,5-triazine (Tz) units into the polymer chain (Fig. 16a). This D–A structure enhances the conjugation of the polymer, reduces the band gap of TzPz, and promotes the transport of electrons along the polymer backbone. The rate performance of BzPz and TzPz was evaluated at different current rates, and the specific capacity gradually decreased with the increase of current rates (Fig. 16b). At current rates of 0.2 A g^{-1} and 5 A g^{-1}, BzPz and TzPz exhibit excellent stability (more than 10 000 cycles) and high specific capacities (TzPz 192 mA h g^{-1}, BzPz 148 mA h g^{-1}) (Fig. 16c and d). *Ex situ* characterization showed that the charge storage of PF_6^- in the TzPz cathode was due to the p-type doping reaction of dihydrophenazine and triazine units (Fig. 16e). These studies suggest that D–A structure design is an effective strategy for the development of high-performance polymer cathodes for DIBs.

In 2023, Liu *et al.*[113] designed and synthesized two CMP materials (CMPs-B and CMPs-By) with spiro-difluorenyl and phenyl groups connected by different bonds (Fig. 17a). However, the CMPs-B materials with monomers linked by C–C bonds have a larger specific surface area of 45 m^2 g^{-1} (CMPs-By: 17 m^2 g^{-1}), smaller microporous size of 1.58 nm (CMPs-By: 2.03 nm), and higher stability in comparison (Fig. 17b and c). This structural feature provides a larger specific surface area in contact with the electrolyte, improves the rapid transfer of Li$^+$ during charging and discharging, retains a certain amount of capacity after multiple cycles (the capacity retention after 100 cycles is 36.6%) and has better multiplicative performance (34.44% for 300 mA g^{-1}) (Fig. 17d and e). This work suggests that increasing the specific surface area of the CMPs is an effective design strategy to improve the electrochemical performance of highly efficient organic electrode materials for LIBs.

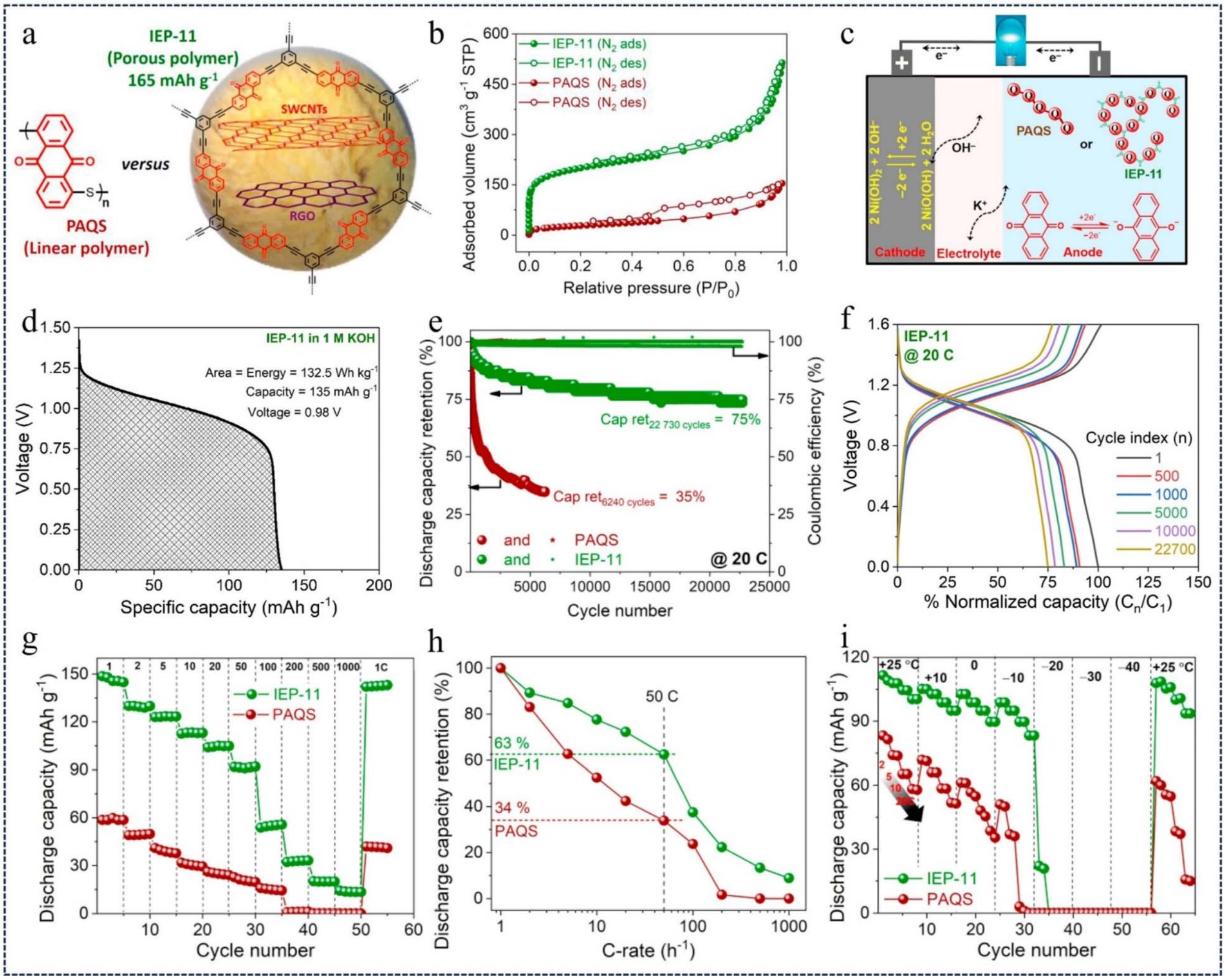

Fig. 13 (a) Chemical structure of PAQS and IEP-11. (b) Nitrogen adsorption–desorption isotherm profiles of PAQS and IEP-11. (c) Schematic of the full cell and its working mechanism. (d) Specific capacity–voltage profile of IEP-11 in 1 M KOH. (e) Cycle stability plot: discharge capacitance retention and coulombic efficiency measured at 20C. (f) Cycle stability plot of IEP-11. (g) and (h) Discharge capacity retention at different C-rates. (i) Low-temperature operativity.[105] Copyright 2022, Elsevier.

Among various organic cathode materials, structures enriched with C═O groups have garnered significant attention globally. Particularly, π-CMPs featuring enriched C═O groups and stable backbones have emerged as a focal point for research efforts. In 2021, Zhai's team[114] synthesized novel CMPs enriched by the bond of C═O utilizing the highly efficient Diels–Alder reaction (Fig. 17f). The resulting CMPs showcase a fused carbon skeleton structure and semiconducting properties, characterized by a band gap of 1.4 eV. Due to their structural properties, the CMPs exhibit good stability (96.1% capacity retention at 0.2 A g^{-1} after 200 cycles and 94.8% capacity retention at 1 A g^{-1} after 1500 cycles), superior lithium-ion diffusion coefficient (5.30×10^{-11} $cm^2\ s^{-1}$) and excellent multiplication capacity (95.8 mA h g^{-1} at 1 A g^{-1}) (Fig. 17g–i). This study broadens the way for the design strategy of CMPs as a cathode material for LIBs.

3.3 CMPs as electrode materials for supercapacitors

Supercapacitors have evolved into prominent energy storage systems for electronic devices due to their high charge/discharge rate, exceptional power density, long cycle life, balanced rate performance, superior cycle efficiency, and environmental friendliness. These properties have garnered significant research interest among scientists and researchers.[115–117] Recently, both organic and inorganic substances have been increasingly utilized as electrodes in supercapacitors. CMPs, in particular, have emerged as attractive electrode materials for capacitors owing to their affordability, chemical stability, flexibility, and widespread availability. They play a pivotal role in enhancing capacitor efficiency.[118–123]

In 2017, Lai *et al.*[124] designed and synthesized the CMPs (TAT-CMP-1, and TAT-CMP-2) with redox activity based on nitrogen-rich and highly conductive triazatriene building blocks as efficient and stable electrode materials for high-performance supercapacitors (Fig. 18a). Due to their favorable porous structure and high nitrogen content, TAT-CMP-1 and TAT-CMP-2 demonstrate high capacitances of 141 F g^{-1} and 183 F g^{-1}, respectively, at a current density of 1 A g^{-1}. Remarkably, they exhibit an ultra-high capacitance per unit surface area

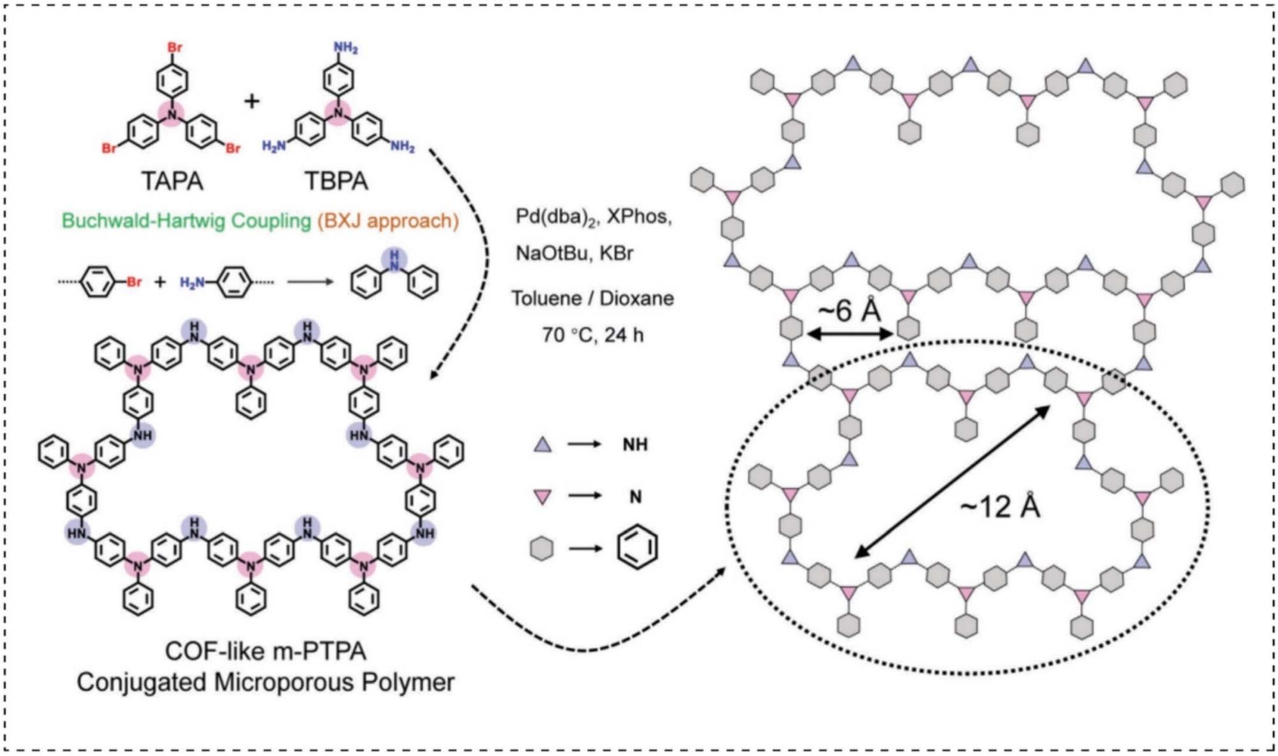

Fig. 14 The synthesis route of COF-like m-PTPA.[106] Copyright 2021, Wiley.

(>160 μF cm^{-2}) (Fig. 18b and c). In addition, TAT-CMP also exhibits excellent reversibility, with cycle efficiencies of 95% and 83% at a high current density of 10 A g^{-1} and after 10 000 cycles, respectively (Fig. 18d). The results show that selectively adjusting nitrogen content by chemical doping is an effective method to improve electrochemical performance.

In 2022, Lai *et al.*[125] developed a set of novel CMPs based on n-type perylene diimide (PDI), namely CMP-1, CMP-2, and CMP-3, as electrode materials for organic capacitors used for flexible energy storage. The morphological characterization showed that they have an irregularly stacked and highly cross-linked morphology, and they have micro- and mesoporous structures (Fig. 19a–c). Given the electron-accepting redox active sites, the hierarchical porous structure, and the amide-linked network, the PDI-CMP electrodes show n-type pseudocapacitive behaviour with high capacity (139–205 F g^{-1} at 0.5 A g^{-1}), wide and negative bias (−1.0–0 V *vs.* Ag/AgCl), and long cycling stability (Fig. 19d and e). Compared to the corresponding CMP-1, CMP-3 features a rigid backbone comprising tetraphenylmethane three-dimensional (3D) structural units and PDI units. This structure promotes ion transfer, increases ionic association, and enhances surface exposure, leading to high specific capacitance, good thermal stability, and excellent reversibility. Notably, CMP-3 exhibits a cycling efficiency of 96% after 5000 cycles at a high current density of 10 A g^{-1} (Fig. 19f). CMP-3 and CMP-2 exhibit faster diffusion kinetics than CMP-1, which can be attributed to the 3D rigid structure of CMP-3 and the twisted molecular structure of CMP-2. Asymmetric supercapacitors employing CMP-3 and poly (3.4-ethylenedioxythiophene)-poly(styrenesulfonate) (PEDOT/PSS) exhibited a wider potential window (1.8 V) and increased capacity (17.4 mF cm^{-2}) compared to symmetric supercapacitors utilizing PEDOT/PSS electrodes. In addition, CMP-3 demonstrates attractive potential as an anode for rechargeable LIBs. This study elucidates a fundamental understanding of the key structural parameters that determine its electrochemical and transport properties, thus opening new doors for the rational design of efficient and stable n-type organic electrode materials for flexible energy storage applications.

In 2018, Liao *et al.*[126] proposed a novel CMP network for energy storage in supercapacitors, a three-dimensional polyaminoanthraquinone (PAQ) network synthesised *via* B–H coupling between 2,6-diaminoanthraquinone (DAQ) and aryl bromides (PAQTA, PAQTB, PAQCB, PAQSF, and PAQTM) (Fig. 20a). PAQ possesses a surface area of up to 600 m^2 g^{-1} and exhibits excellent dispersion in polar solvents, making it suitable for processing into flexible electrodes. Notably, PAQTA demonstrated a specific capacitance of 576 F g^{-1} (three-electrode configuration) in 0.5 M H_2SO_4 at a current density of 1 A g^{-1}. Furthermore, it maintained 80–85% capacitance over 6000 cycles at a current density of 2 A g^{-1}, with a nearly 100% coulombic efficiency (95–98%) (Fig. 20b–e). Asymmetric two-electrode supercapacitors assembled from PAQs show a total electrode material capacitance of 168 F g^{-1}, an energy density of 60 W h kg^{-1} at a power density of 1300 W kg^{-1}, and a wide operating potential window (0–1.6 V). The asymmetric supercapacitor has a coulombic efficiency of 97% and maintains

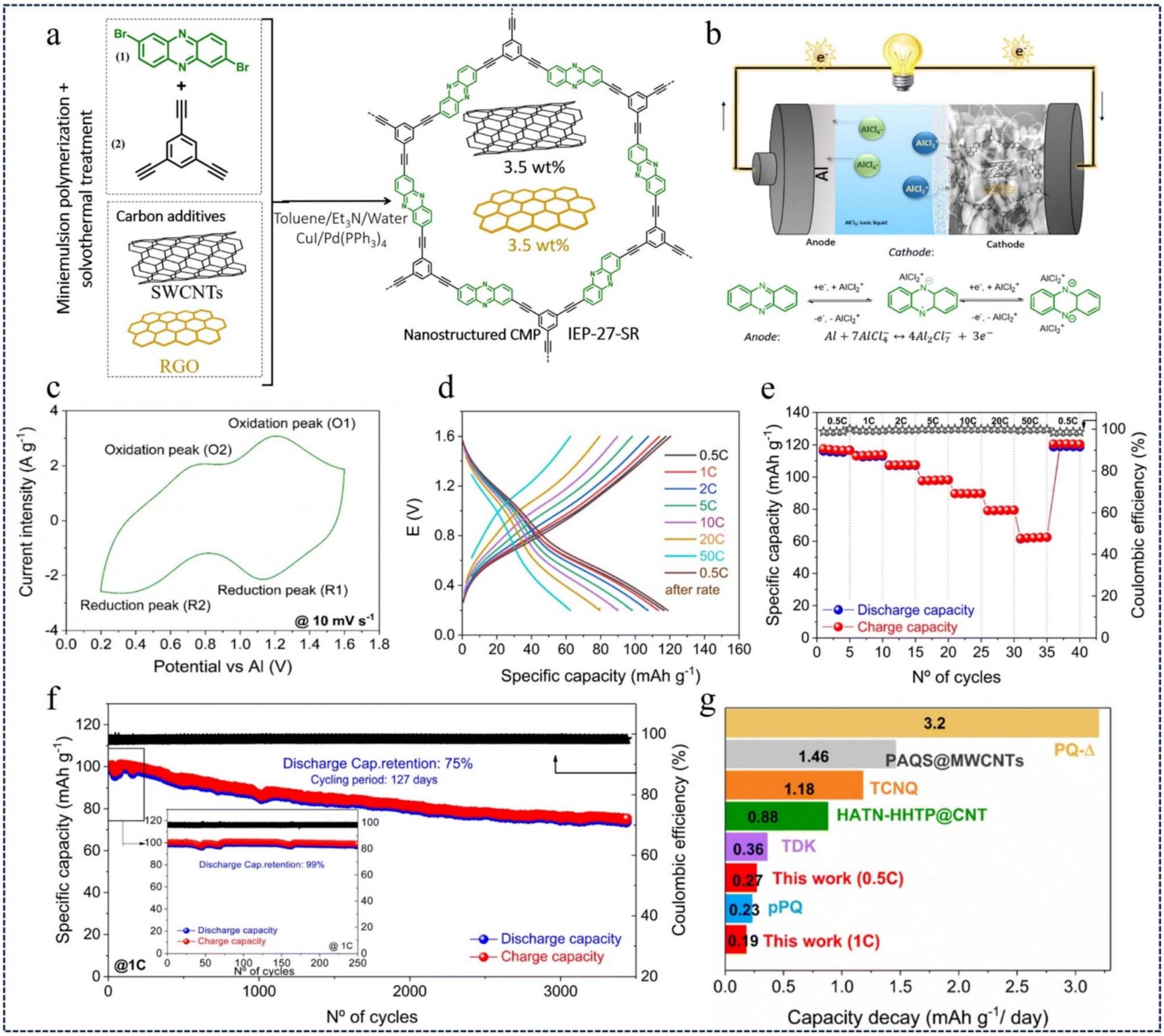

Fig. 15 (a) Synthesis strategy for IEP-27-SR mixtures. (b) Scheme of the aluminium–phenazine battery. (c) CV recorded at 10 mV s^{-1}. (d) GCD profiles of the Al//IEP-27-SR battery. (e) Battery rate performance. (f) Long-term cycle stability of an Al//IEP-27-SR battery. (g) Capacity fade per day.[107] Copyright 2023, Royal Society of Chemistry.

95.5% of its initial capacitance under 2000 cycles (Fig. 20f). This work presents new promising CMP networks for charge storage.

Fiber-based supercapacitors (FSCs) are a promising energy storage device to meet the growing demand for miniaturization, flexibility and compatibility in wearable electronic devices.[127,128] However, low energy density compared to batteries remains a major limitation for practical applications.[129,130] In 2020, Liao *et al.*[131] utilized various amine monomers (aniline, pyridine, and anthraquinone) along with 1,3,5-tris(3-bromo)-benzene (TPBA) monomers, which were polymerized on the surface of a carbon nanotube fiber (CNF) through a B–H cross-coupling reaction. This process yielded a CMP network (CNF@CMP) characterized by a tailorable porous structure and reversible redox chemistry (Fig. 21a), exhibiting highly efficient capacitive properties. Due to the flexibility and high conductivity of CNFs, along with the porosity and strong redox properties of the polytriphenylamine network structure (PTPA), as well as the enhanced synergistic interaction between the CNF core and PTPA shell, it is used to prepare high-performance wearable supercapacitors (671.9 mF cm^{-2} at a current density of 1 mA cm^{-2}). All-solid-state symmetrically twisted CNF@PTPA FSCs prepared with PVA/H_3PO_4 as the gel electrolyte exhibited a high specific surface area capacitance of 398 mF cm^{-2} (0.28 mA cm^{-2}) (Fig. 21b and c), a maximum operating voltage of 1.4 V, and an energy density of 18.33 μWh cm^{-2} (Fig. 21d). In addition, they exhibit excellent flexibility and mechanical stability, maintaining 84.5% of the initial capacitance after 10 000 bending cycles (Fig. 21e). These materials provide a new avenue for high-performance wearable supercapacitors (HPWS) with a wide range of potential applications in wearable electronics.

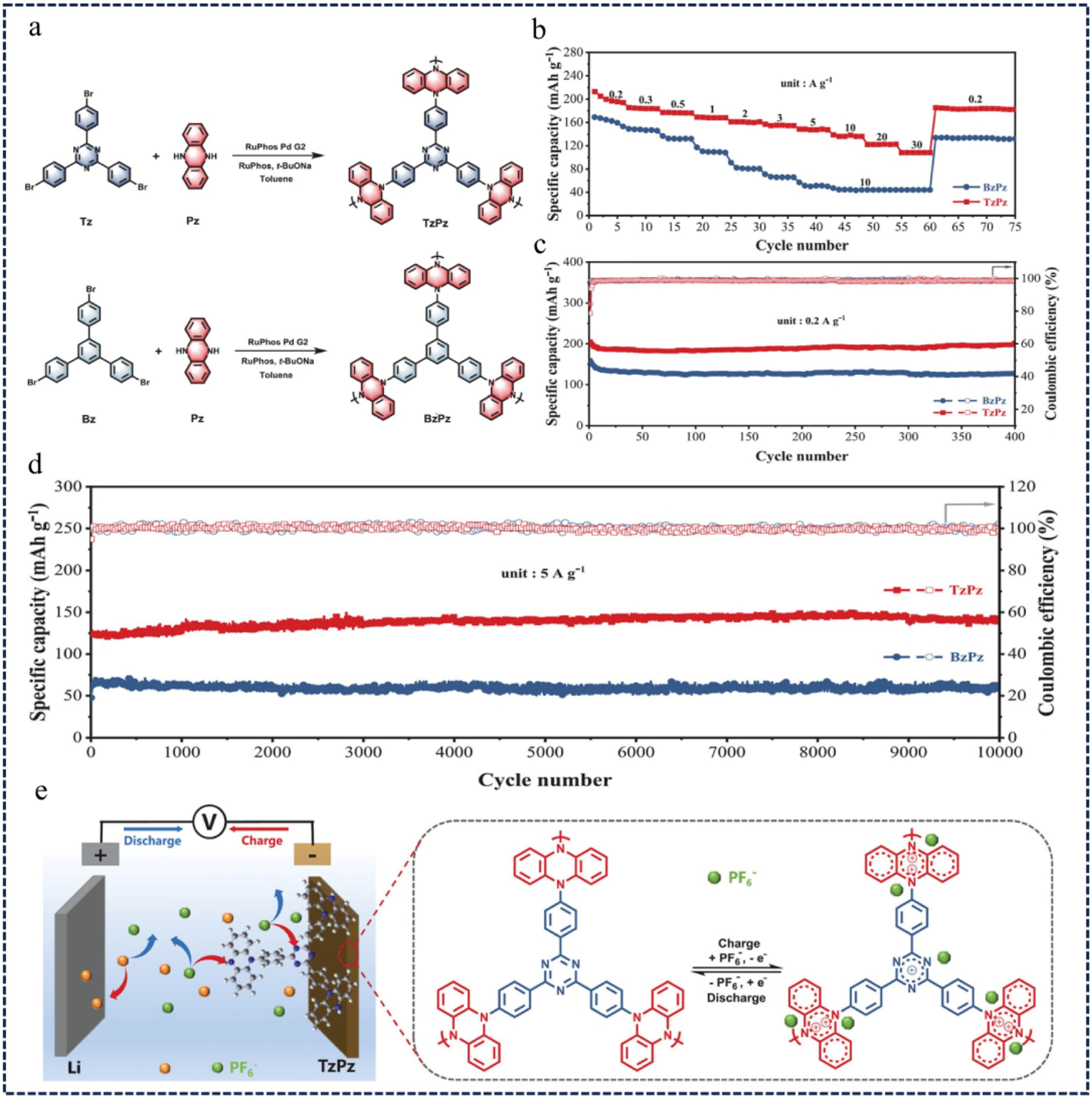

Fig. 16 (a) The synthetic reaction route of TzPz and BzPz. (b) The rate performance at current densities from 0.2 to 30 A g^{-1}. (c) Cycling performance at current densities of 0.2 A g^{-1} and (d) 5 A g^{-1}. (e) Schematic diagram of the electrochemical reaction mechanism of the TzPz-based cathode.[112] Copyright 2021, Wiley.

CMPs with active functional groups have received increasing attention in energy conversion systems.[132,133] However, their low conductivity results in low capacitance, which limits their practical applications.[134,135] In 2021, Duan *et al.*[136] designed and synthesised CMPs comprising trityl aldehydes linked to metal phthalocyanines (MNC, Co, and Fe). Composite membranes were prepared by combining them with highly conductive CNTs in different ratios (MNC : CNT = 1 : 1, 1 : 2, 1 : 3, and 1 : 5) using a microwave method and vacuum filtration strategy. These composite membranes are denoted as MNCCs-x, where $x = 1, 2, 3, 5$ (Fig. 22a). Due to the highly active metallic properties of CoNC, it can be compounded with highly conductive CNTs through π–π interactions without any covalent bonding into CoNCCs. These CoNCCs are flexible and can serve as self-supporting, binder-free flexible electrodes for supercapacitors. The optimized CoNCCs-3 flexible electrodes exhibit a high specific capacitance of 213.4 F g^{-1} at a current of 0.5 A g^{-1} (Fig. 22b). In addition, a capacity retention of 85.3% was achieved after 1750 cycles at 20 A g^{-1} (Fig. 22c). The good electrochemical performance can be attributed to the synergistic effect and strong biphasic interaction between MNC and CNTs. This work opens the way for the development of high-performance

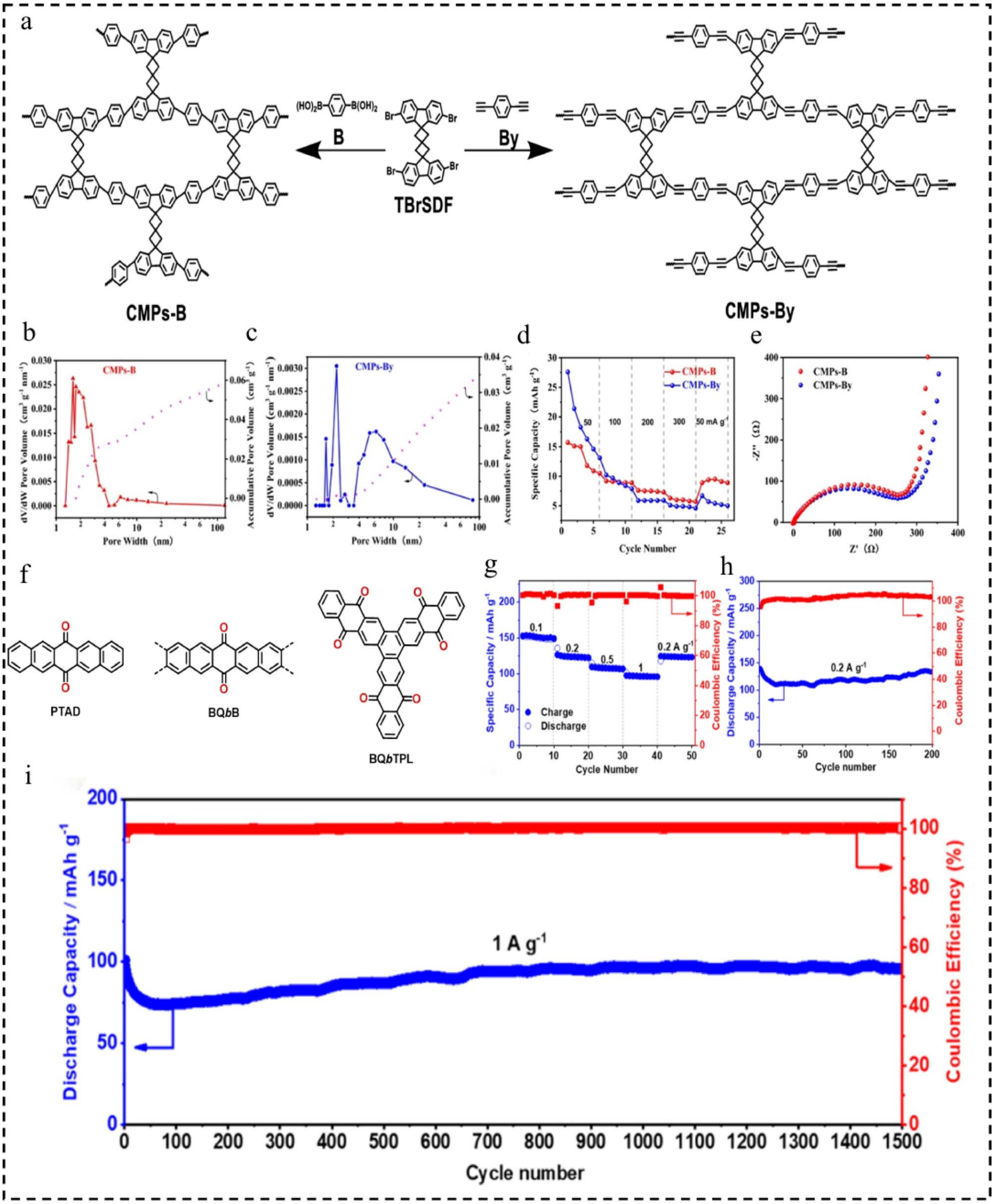

Fig. 17 (a) Synthesis of CMPs-B and CMPs-By. (b) Pore size distribution curve (red) and cumulative pore volume curve (pink) of CMPs-B. (c) Pore size distribution curve (blue) and cumulative pore volume curve (pink) of CMPs-By. (d) Rate performance of the CMP-based electrode at different current densities. (e) Nyquist plots of the pristine and CMP-based electrode.[113] Copyright 2023, Springer. (f) The structure of PTAD, BQbB, and BQbTPL. (g) Rate capability at different current densities and cycle performance at (h) 0.2 A g^{-1} and (i) 1.0 A g^{-1}.[114] Copyright 2021, American Chemical Society.

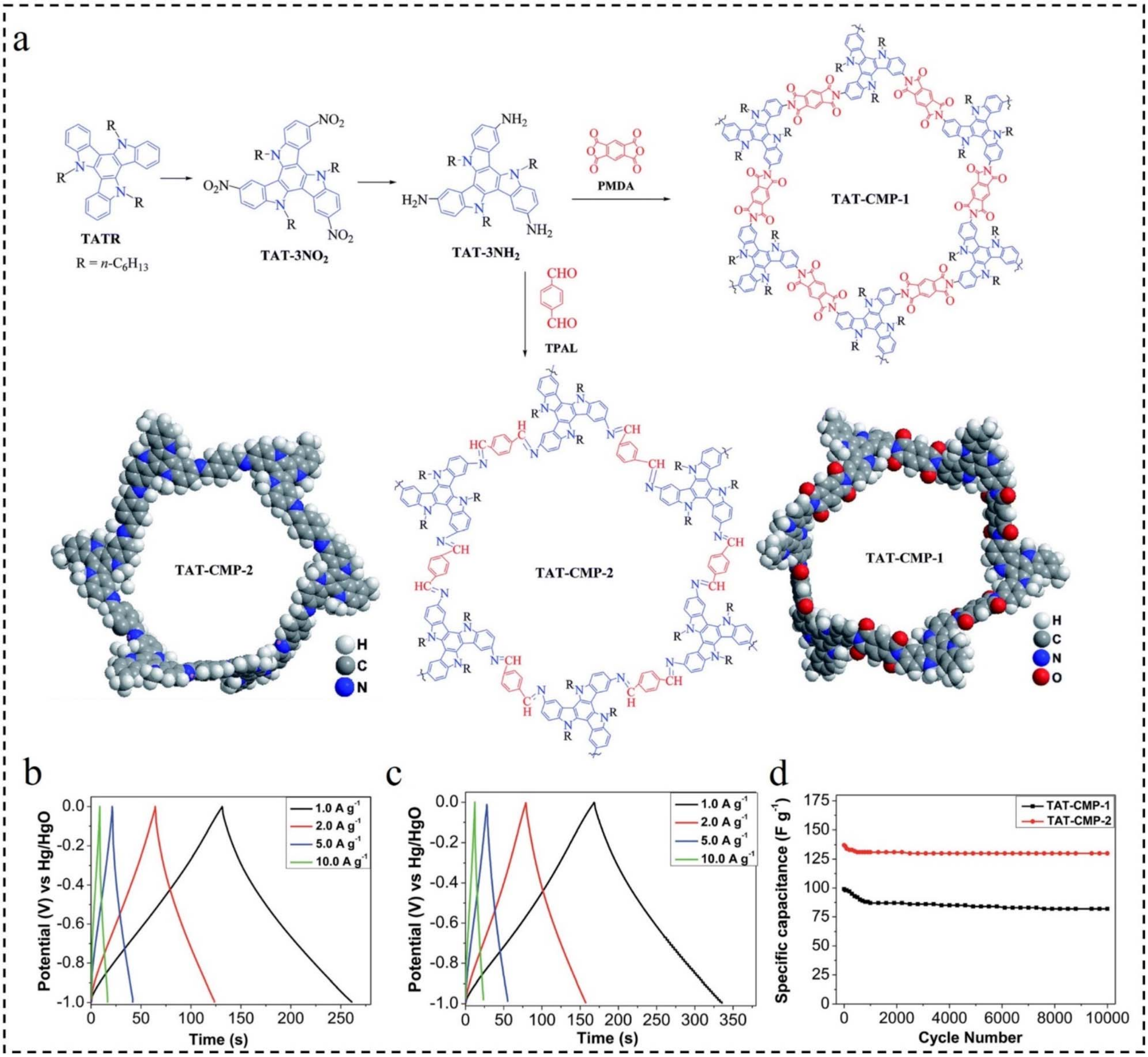

Fig. 18 (a) The structure of TAT-CMP-1 and TAT-CMP-2. GCD curves of (b) TAT-CMP-1 and (c) TAT-CMP-2 at different current densities. (d) The relationship of the specific capacitance with cycling number for TAT-CMP-1 and TAT-CMP-2 at a current density of 10 A g^{-1} after 10 000 cycles.[124] Copyright 2017, Royal Society of Chemistry.

organic supercapacitor electrode materials with a low environmental footprint.

Metal phthalocyanines (MPcs), an important functional π-conjugated structural unit, are two-dimensional aromatic molecules containing a metal at the centre of the inner ring, and MPcs exhibit excellent electron-transfer ability due to the interaction between the phthalocyanine ring and the metal centre.[137–140] MPc-based CMPs may have potential applications in energy conversion and storage systems.[141] In 2020, Duan *et al.*[142] fabricated three MPc-based CMPs (M = Co, Fe, and H_2) using a rapid microwave method. Subsequently, they hybridized MPc-CMPs with CNTs to produce free-standing and flexible composite membranes through non-covalent bonding. These composite membranes serve as flexible electrodes for supercapacitors without the need for additives or binders (Fig. 22d). Due to the synergistic effect and strong π–π interaction between the MPc-CMP and CNTs, the flexible electrodes CoPc-CMP/CNTs-2, HPcCMP/CNTs-2 and FePc-CMP/CNTs-2 showed high specific capacitances of 289.1 F g^{-1}, 53.6 F g^{-1} and 100.7 F g^{-1} at a current density of 1 A g^{-1}, respectively (Fig. 22e). Even at a current density of 10 A g^{-1}, CoPc CMP/CNTs-2 can show a high specific capacitance of 107.2 F g^{-1} and a high specific capacitance retention rate of 89.2% after 1350 cycles (Fig. 22f). The study shows that the synergistic effect and powerful functions of metal phthalocyanine-linked CMPs and highly conductive CNTs open up the possibility of developing high-performance supercapacitors.

Porphyrin-based CMPs have great potential for applications in energy storage systems, but their low conductivity limits their practical applications.[143,144] To address this issue, in 2021, Duan

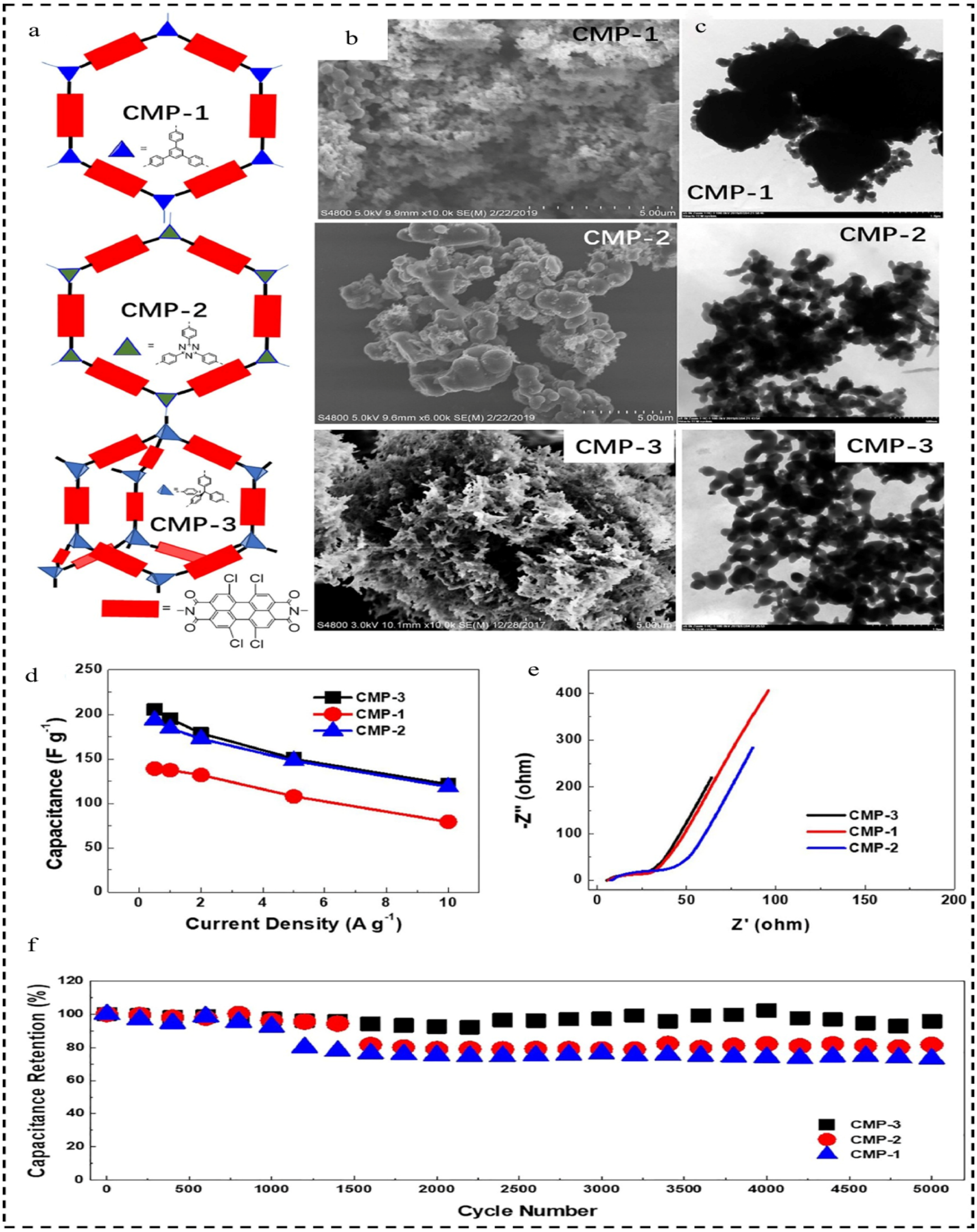

Fig. 19 (a) Graphic representation of CMP-1, CMP-2 and CMP-3. (b) SEM images of CMP-1, CMP-2 and CMP-3. (c) TEM images of CMP-1, CMP-2 and CMP-3. (d) Specific capacitance *versus* current density curve of CMP-1, CMP-2 and CMP-3. (e) Nyquist plot of CMP-1, CMP-2 and CMP-3. (f) Cycling stability of CMP-1, CMP-2 and CMP-3 at a current density of 10 A g^{-1}.[125] Copyright 2022, Springer.

et al.[145] introduced a solution by designing and synthesizing copper porphyrin-CMPs (CuTAPP-CMPs). They further created CuTAPP-CMP/CNTs-3 by integrating CuTAPP-CMPs with highly conductive CNTs through a straightforward vacuum filtration method (Fig. 23a). These materials serve as non-adhesive, standalone flexible electrodes for supercapacitors. In the absence of any covalent bonding, the active CuTAPP-CMP can bind to the conducting CNTs in view of the π–π interactions. The flexible electrode of CuTAPP-CMP/CNTs-3 exhibits a specific capacitance of 207.8 F g^{-1} at 1 A g^{-1} (Fig. 23b) and

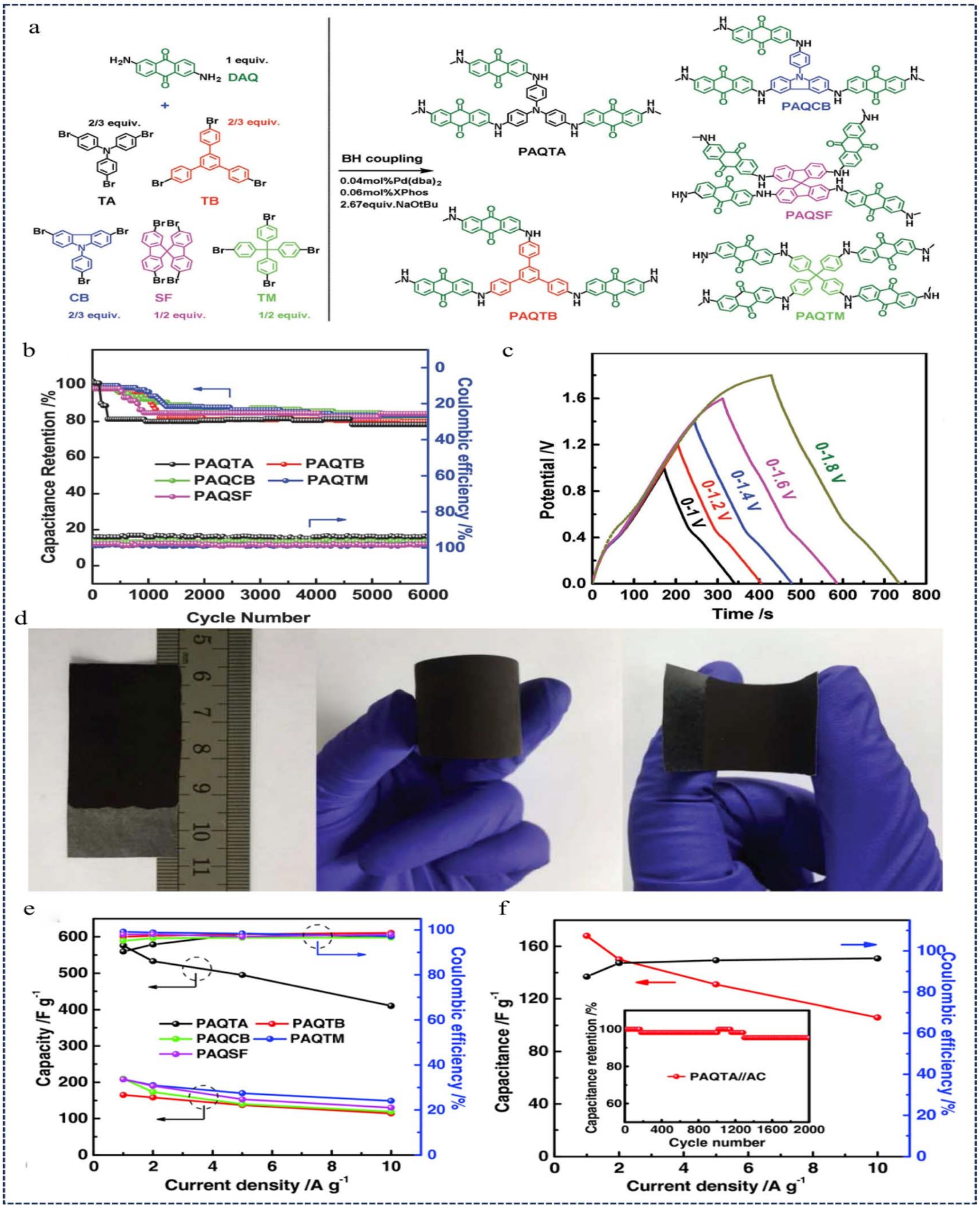

Fig. 20 (a) Synthetic routes of PAQTA, PAQTB, PAQCB, PAQSF, and PAQTM. (b) Cyclability tests and coulombic efficiencies of PAQs. (c) GCD curves at a current density of 1.0 A g^{-1}. (d) Photographs of flexible PAQTA electrodes and electrochemical performance of PAQs obtained in 0.5 M H_2SO_4. (e) Specific capacitance and coulombic efficiency of PAQs obtained at different current densities. (f) Specific capacitance and its retention as well as the coulombic efficiency based on the total mass of the two electrodes *versus* current density with the inset showing the cycle durability of the device at a current of 2.0 A g^{-1}.[126] Copyright 2018, Wiley.

a long cycling performance of more than 3700 cycles at 20 A g^{-1} (Fig. 23c). The impressive electrochemical performance observed can be attributed to the synergistic effect of the high electrical conductivity of CNTs combined with the high pseudocapacitance of CuTAPP-CMP. This study paves the way for the exploration of high-performance organic active materials for supercapacitors.

In 2022, Mohamed *et al.*[123] constructed three 1,3,4-oxadiazole-CMPs (OXD-CMPs: TPA-OXD-CMP, Py-OXD-CMP, and TPE-OXD-CMP) by simple Sonogashira coupling. CNTs were combined with OXD-CMPs using non-covalent bonding π–π interactions to provide OXD-CMPs/CNTs composites (Fig. 23d). When used as electrodes for supercapacitors, they have greatly enhanced capacitance and cycling stability, where

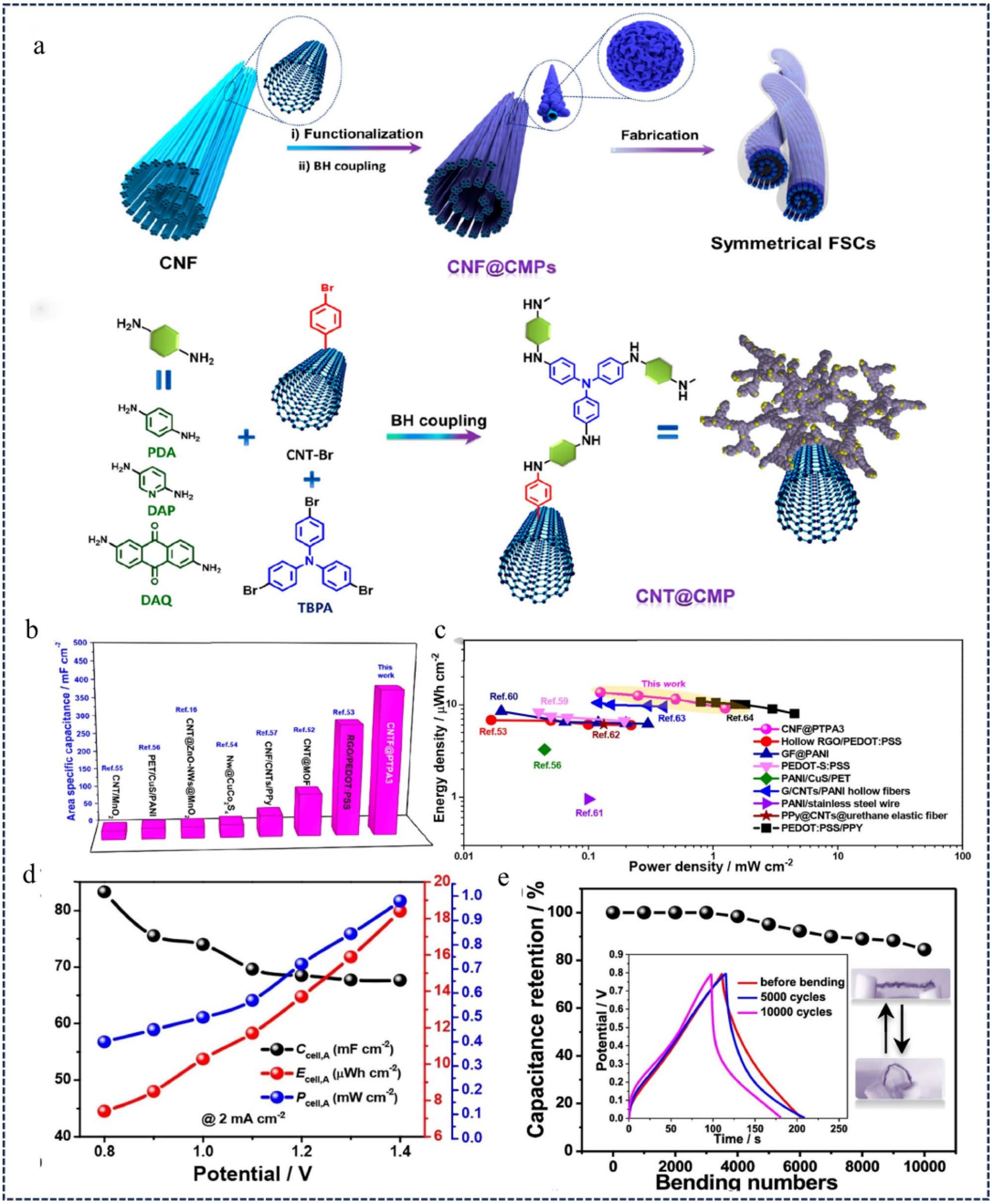

Fig. 21 (a) Schematic illustration of the fabrication process for symmetrical fiber-shaped supercapacitors (FSCs). (b) Areal Ragone plots of the CNF@PTPA-based FSCs. (c) Comparison of electrochemical performance of CNF@PTPA FSCs with other FSCs in terms of specific capacitance. (d) GCD curves of CNF@CMP fibers. (e) Relationship between capacitance retention and bending times.[131] Copyright 2020, American Chemical Society.

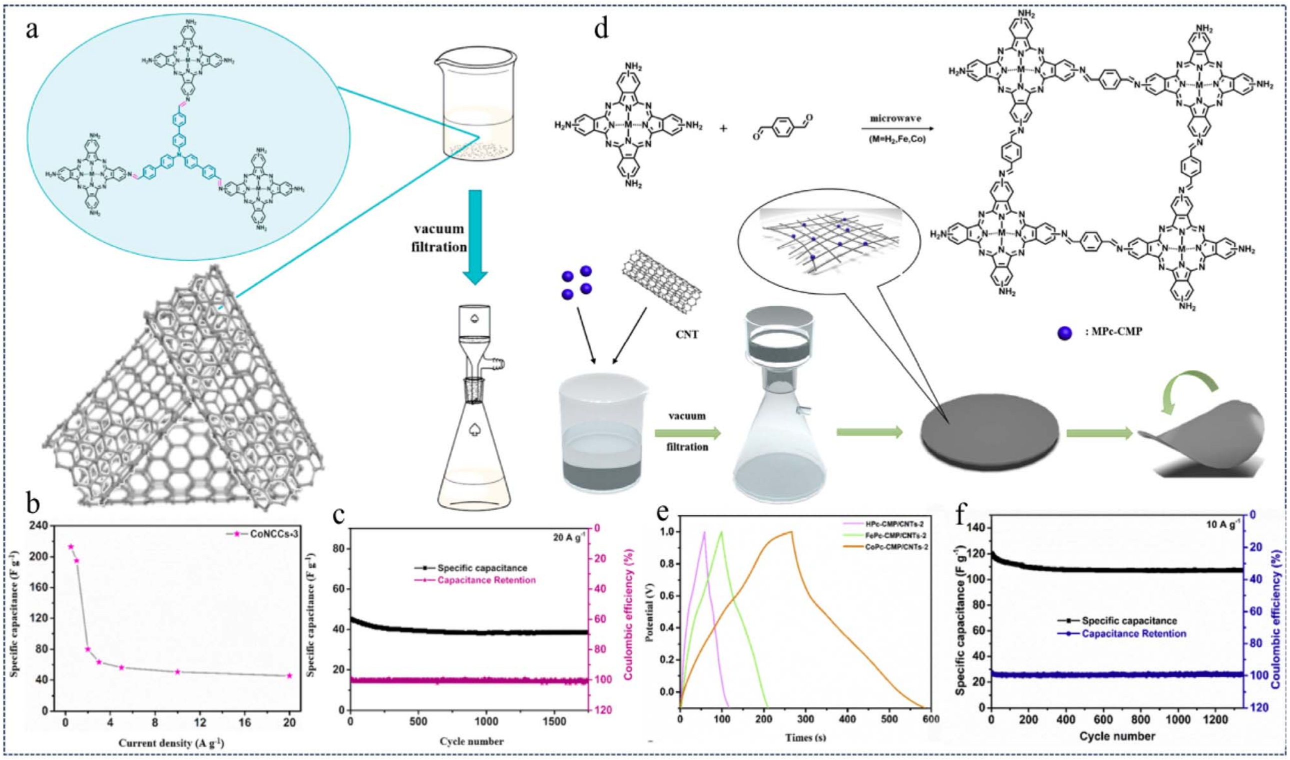

Fig. 22 (a) Schematic preparation process for MNCCs (M = Co, Fe). (b) Specific capacitances of CoNCCs-3 at different current densities. (c) Cycling performance and coulombic efficiency of CoNCCs-3 at 20 A g^{-1}.[136] Copyright 2021, Elsevier. (d) Synthetic process of MPc-CMP/CNTs. (e) GCD curves of MPc-CMP/CNTs-2 (M = H_2, Co, Fe) obtained at 1 A g^{-1}. (f) Cycling performance and coulombic efficiency of CoPc-CMP/CNTs-2 at 10 A g^{-1}.[142] Copyright 2020, Elsevier.

the capacity of the Py-OXD-CMP/CNT composites is 504 F g^{-1} at a current density of 0.5 A g^{-1}, which is much higher than that of other OXD-CMP-based samples. The Py-OXD-CMP/CNT composite exhibits excellent cycling stability (91.1% capacitance retention) as measured by GCD for 2000 cycles at a current density of 10 A g^{-1} (Fig. 23e and f). The results show that OXD-CMPs/CNTs nanocomposites are promising for high-performance charge storage.

In 2023, Gaber *et al.*[146] synthesised unique redox-active CMPs, Py-BDT and Py-Ph-BDT-CMPs. Such CMPs are based on pyrene (Py) and redox-active benzo[1,2-*b*:4,5-*b*′] dithiophene-4-one (BDT) units, and act as highly efficient and stable electrodes for supercapacitor energy storage devices. CMPs exhibit excellent thermal stability (T_{d10}: ∼564 °C; coke yield: ∼70.5%) and surface area (∼427 m^2 g^{-1}). At a current density of 0.5 A g^{-1}, Py-BDT and Py-Ph-BDT CMPs exhibit excellent three-electrode capacitance of 636 and 712 F g^{-1}, respectively, which is better than the previously reported specific capacitance of conventional CMPs. Symmetric two-electrode supercapacitors constructed with Py-Ph BDT CMPs showed an effective capacitance of 429 F g^{-1} and an energy density of 38.21 W h kg^{-1} at a potential of 0.8 V and maintained 80% of their initial capacitance over 4000 cycles (Fig. 23g–i). It was found that the redox process of such CMPs mainly depends on the BDT monomer, which is reduced using two electrons during discharge, whereas the reversible oxidation of the BDT^{2-} anion occurs continuously during the charging phase, and thus the integration of the pyrene and BDT monomers into CMP cores could lead to fast charge transfer, excellent Faraday energy storage, and remarkable electrical conductivity (Fig. 23j). This work presents a new strategy for the preparation of high-capacity supercapacitors from reducible CMPs.

In 2022, Jang *et al.*[147] prepared a conjugated microporous anthraquinone amide polymer network (CMAP@AG) with electron-transporting properties by a simple one-step B–H coupling of anthraquinone amide and tris-aniline as the basic polymerization units on an activated graphene substrate (Fig. 24a). The structural properties of the CMAP@AG composites were optimized by varying the etching time of the AG substrate material (Fig. 24b), exhibiting up to 751 F g^{-1} (Fig. 24c) at a current density of 1.0 A g^{-1} and maintaining 97% of the initial capacitance after 20 000 effective cycles after increasing the current density to 10.0 A g^{-1} (Fig. 24d). In addition, the asymmetric supercapacitors assembled from CMAP@A4G exhibit a high energy density of 76.6 W h kg^{-1} and a high-power density of 27 634 W kg^{-1} in the voltage range of 0–1.5 V. Moreover, the composite CMP network is capable of bending and has certain mechanical strength, which is a better flexible CMP composite material. This study demonstrated through extensive experiments that CMAP@A4G has high redox activity, good electrochemical properties and stable cyclability, and the surface area of the composite can reach up to 498 m^2

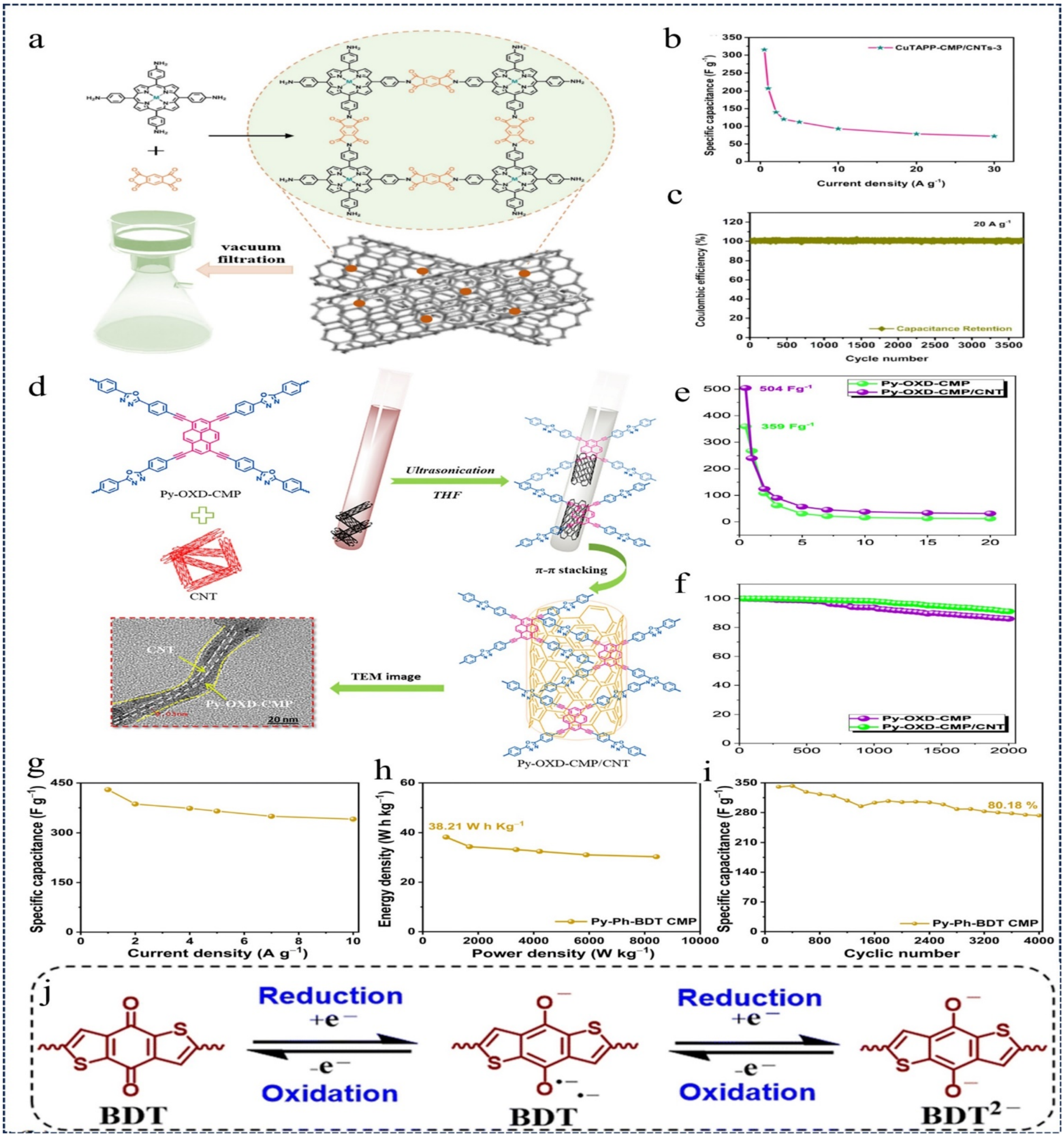

Fig. 23 (a) Schematic preparation process for MTAPP-CMP/CNTs (M = Cu and H_2). (b) Specific capacitances of CuTAPP-CMP/CNTs-3 at different current densities. (c) Coulombic efficiency of CuTAPPCMP/CNTs-3 at 20 A g^{-1}.[145] Copyright 2021, Springer. (d) Schematic synthesis of the Py-OXD-CMP/CNT nanocomposite. (e) Specific capacitances of the Py-OXD-CMP and Py-OXD-CMP/CNT nanocomposites. (f) Stability profiles of the Py-OXD-CMP and Py-OXD-CMP/CNT nanocomposites.[123] Copyright 2022, American Chemical Society. (g) Calculated specific capacitances of the Py-Ph-BDT CMP tethered supercapacitor. (h) Ragone plot of energy density *versus* power density for the Py-Ph-BDT CMP-tethered supercapacitor. (i) Cycling performance of the Py-PhBDT CMP-tethered supercapacitor at a current density of 5 A g^{-1}. (j) Redox mechanism of the BDT unit.[146] Copyright 2023, Royal Society of Chemistry.

g^{-1}. This study provides insights into the rational design and effective regulation of CMP-based active graphene composites for energy storage devices.

CMPs are usually obtained as amorphous or semi-crystalline powders, taking into account the fact that electrostatic spinning is a well-established and versatile technique for the fabrication of nanofibres with diameters ranging from tens of nanometers to a few micrometres, which are usually highly flexible and have a high surface area-to-volume ratio, which is conducive to the fabrication of chemosensor devices with a fast response and

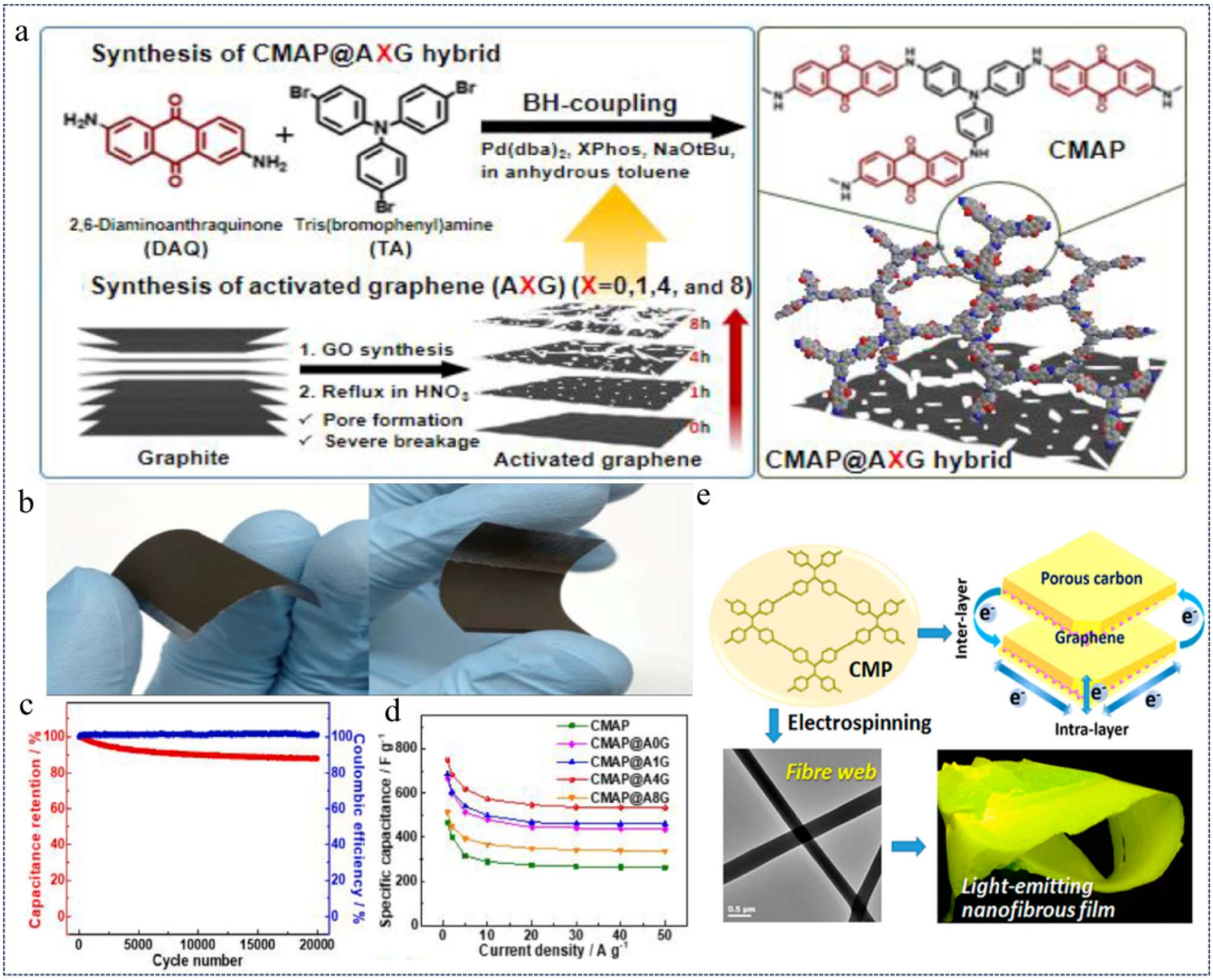

Fig. 24 (a) Synthesis of the CMAP@XG hybrid. (b) Photographs of flexible CMAP@A4G electrodes. (c) Specific capacitance obtained at different scan rates from 1 to 50 A g^{-1}. (d) Capacitance retention and coulombic efficiency test charts at a current density of 10 A g^{-1}.[147] Copyright 2022, Elsevier. (e) Schematic diagram of electron transfer in graphene templated CMPs.[41] Copyright 2015, American Chemical Society.

a high sensitivity.[39,148,149] In 2015, Chen and his team[41] prepared CMP materials by the Sonogashira coupling reaction using tetraaryl ethylene as the polymerization unit, and prepared a sensitive sensor with high flexibility, high porosity and surface area-to-volume ratio, and suitable for the detection of nitroaromatics and benzoquinone vapours, as well as oxidising metal ions, by efficiently mixing the CMPs with PLA by means of electrostatic spinning (Fig. 24e). Furthermore, sandwich structures comprising graphene-based CMPs (G-CMPs) boast high surface area and aspect ratio properties. These structures can be synthesized *via* pyrolysis at 800 °C to yield hierarchical porous carbon-rich 2D carbon nanosheets. Remarkably, these carbon nanomaterials demonstrate exceptional supercapacitor performance, showcasing a 48% increase in capacitance compared to porous carbon without graphene templates. The introduction of graphene scaffolds facilitates efficient inter/intralayer electron transport, which improves ion injection/extraction from or to the electrodes and enhances energy storage capacity.

3.4 CMPs as other flexible materials

CMP materials are excellent across various fields owing to their unique structure and large specific surface area, among other advantages. However, the formation of rigid π-conjugated networks renders them insoluble in most organic solvents, resulting in poor processability and limitations in certain practical applications. To address these scientific challenges and expand the application scope of CMP materials, researchers have shown considerable interest in developing CMP flexible membranes.

Membranes with fast and selective ion transport have great potential for water and energy-related applications, and the structural and material design of membranes plays a key role in improving their performance.[150] In 2021, Lai *et al.*[151] prepared two flexible ionic CMP films (i-CMP and n-CMP) with adjustable thickness by co-electro polymerization (Fig. 25a). Unlike conventional CMP film materials, the Young's modulus of the two films averages 4 GPa (Fig. 25b), and the specific surface

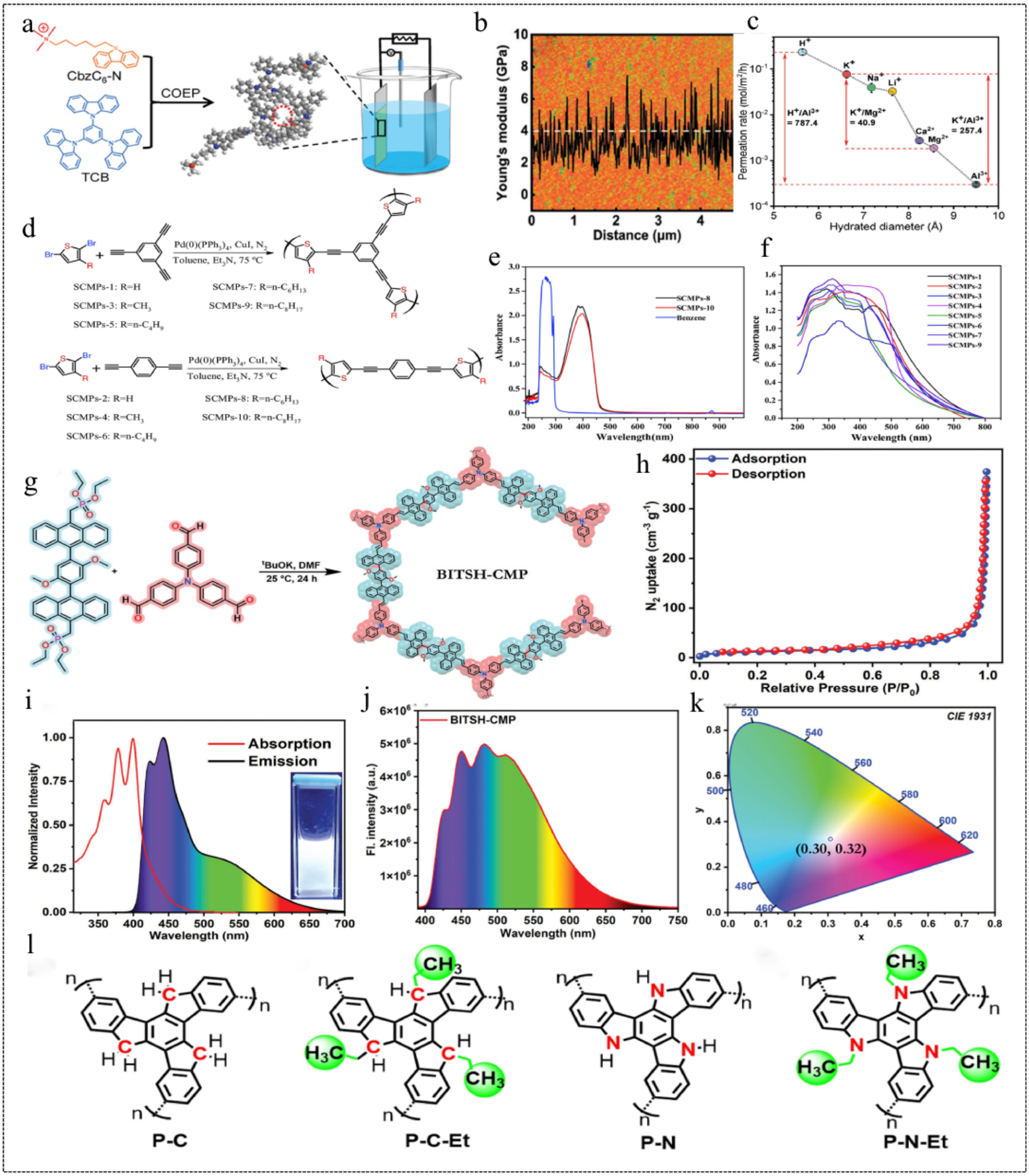

Fig. 25 (a) Schematic diagram of the i-CMP membrane prepared by co-electrolytic polymerization. (b) AFM image of CMP membranes. (c) Selective ion permeation of the i-CMP membrane.[151] Copyright 2021, Wiley. (d) Representative molecular structure of the repeat units for SCMPs. (e) Ultraviolet-visible absorption spectra of SCMPs-8 and SCMPs-10 in chloroform solution. (f) Solid-state ultraviolet-visible absorption spectra of SCMPs.[152] Copyright 2018, Wiley. (g) Synthetic method for BITSH-CMP. (h) N_2-isothermal adsorption curve at 77 K. (i) Normalised absorption and fluorescence spectra of BITSH-CMP. (j) Fluorescence spectra of BITSH-CMP blended with PVA. (k) CIE plot.[153] Copyright 2023, Wiley. (l) The molecular structures of the CMPs.[154] Copyright 2021, Elsevier.

areas of i-CMP and n-CMP are 821 $m^2\ g^{-1}$ and 773 $m^2\ g^{-1}$, respectively. Due to the introduction of soft carbon chains into the CMP monomer, the thin film structure has dual flexibility and functional control. The selectivity of the two CMP films for H^+/Mg^{2+} was 9.3 (i-CMP) and 2.5 (n-CMP), respectively, during the electrically driven process. In the concentration-driven process, the selectivity of i-CMP and n-CMP for K^+/Mg^{2+} is 7.1 and 40.9 (Fig. 25c), respectively, which is better than that of the commercially available Nafion 117 in both driving modes. This study provides a new idea for the fabrication of flexible CMP films.

In 2018, Ren *et al.*[152] prepared a series of soluble flexible CMP materials (SCMPs). A significant improvement in the solubility of SCMPs was achieved by adjusting the length of the alkyl chains in the alkyl-substituted dibromothiophene monomers (Fig. 25d). The BET specific surface areas of SCMPs-1, SCMPs-2, SCMPs-3, and SCMPs-4 were determined to be 182.18 $m^2\ g^{-1}$, 32.12 $m^2\ g^{-1}$, 1.86 $m^2\ g^{-1}$, and 4.70 $m^2\ g^{-1}$, respectively. Notably, the pore size distribution (PSD) for SCMPs-1 exhibited a narrower distribution, with a pore size of only 12.79 nm, this suggests that the introduction of alkyl chains in the monomer leads to a decrease in the BET specific surface area. The SCMP samples have a strong UV absorption and fluorescence effect. At optimal excitation wavelengths, these polymers, characterized by short carbon branches (no more than 4 carbon atoms) or no alkyl substitutions, emit blue and green fluorescence for SCMPs-1 and SCMPs-6, respectively. Conversely, samples featuring longer carbon branches ($n_C = 6$ or 8), spanning from SCMPs-7 to SCMPs-10, emit blue fluorescence (Fig. 25e). Functional composite flexible films of SCMPs were formed on a number of different soft and hard substrates using spin-coating, substrate casting and dip-coating methods, and these soluble SCMP samples can be used as functional coatings with some UV protection due to their strong UV absorption at 250 and 380 nm (Fig. 25f). The results revealed that both SCMP-coated PDMS films exhibited outstanding optical transparency in the visible region (>75% from 450 to 780 nm). However, the UV transmittance of the as-prepared SCMP-coated PDMS films at 357 nm was observed to be only 39.26% (SCMPs-8-PDMS) and 26.70% (SCMPs-10-PDMS), respectively. In conclusion, it was found that the structure and composition of the monomers can be fine-tuned to provide new possibilities for the rational design of novel CMP materials with desired functionality and porosity.

In 2023, Prusti *et al.*[153] quantitatively obtained a newly designed CMP (BITSH-CMP) by the Horner–Wadsworth–Emmons reaction (Fig. 25g). The CMP was characterized by conformational distortions and electron-rich two-state white light emission, and had a specific surface area of up to 248 $m^2\ g^{-1}$ with a pore size of 1.76 nm (Fig. 25h). This CMP emits an intense white light in solution, produces yellow emission in the solid state, and when mixed with polyvinyl alcohol, produces a flexible, intense white light emission in the film. BITSH-CMP uses the electron-rich TPA nucleus (TPA2A) as a donor and the anthracene nucleus (An2P2) as an acceptor, allowing the intramolecular charge transfer process to proceed smoothly. The tuning of the white emission can be scrutinised by varying the concentration of the CMP (Fig. 25i and j), and the solution white emission can be tuned by adjusting the concentration in dimethylsulphoxide [CIE: 0.29, 0.32], and the flexible film produces white emission (CIE: 0.30, 0.32) (Fig. 25k). This CMP is currently under investigation for solid-state device fabrication, involving its blending with commercially available, electron-rich polyvinyl alcohol to enhance its intramolecular charge transfer (ICT) process. This results in the formation of a flexible white light emitter (WLE) with significant strength. This robust and accessible flexible device emits strong white light, expanding the practical applications of solid-state white light emitting materials.

CMPs with rigid π-conjugated backbones and tunable microporous structures show great potential as gas storage and sequestration materials.[18] In 2021, Zhu *et al.*[154] prepared flexible alkyl@rigid containing backbone CMPs (P-C(-Et) and P-N(-Et)) based on truxene and triazatruxene, which are highly gas-absorbent (Fig. 25l). The results suggest that incorporating rational flexible moieties with additional rigid backbone structures can induce a transformation of the 2D C3 symmetric structural core into a 3D stereoscopic configuration. Gas adsorption measurements further indicate that alkyl@rigid incorporated CMPs are likely to exhibit higher surface areas (ranging from 339 to 1031 $m^2\ g^{-1}$ for truxene and from 324 to 1150 $m^2\ g^{-1}$ for triazatruxene) and narrower pore size distributions. The optimized molecular structures exhibit a high CO_2 uptake capacity, ranging from 5.8 to 11.5 wt% for turquoise and 7.8–17.6 wt% for triazapatite at 273 K and 1.0 bar. Furthermore, these optimized structures demonstrate superior selectivity for CO_2 even in the presence of N_2 or CH_4 in the system. In conclusion, this work provides a fundamental understanding of the design of CMPs with high CO_2 adsorption and separation performance.

4 Conclusions and perspectives

CMPs, as an important part of the porous organic polymer family, have a unique microporous π-conjugated backbone and also represent a future multifunctional platform. CMPs have numerous applications for electrode energy storage due to their high redox activity, excellent physicochemical stability, highly crosslinked polymer network, rich porous structure and large surface area. As smart and flexible electronic devices have gradually become the trend of the future, CMP flexible electrodes are becoming a new area of scientific interest. It is possible to adjust the composition, internal morphological structure and performance of the organic modules by optimising the molecular design to meet the requirements of a specific application, and the research on CMP flexible electrodes is moving towards the direction of low-cost, high-energy density, high power density, and long cyclic life.

In this review, we systematically demonstrate a variety of CMP construction methods and applications in flexible electrodes, which mainly have the following problems: (1) many coupling reactions require the introduction of transition metal catalysts, which may have unclean catalyst treatment, blocking the pores of CMPs and affecting the electrochemical performance of CMPs. (2) In the metal-free catalytic system, CMPs with complex structures are difficult to prepare and cannot be produced on a large scale. (3) In the natural state, CMPs exist in a powder or semi-crystalline state, which is difficult to process.

Therefore, based on the above problems, researchers should consider in-depth research on the development and application of flexible electrodes based on CMPs in the future, mainly in the following aspects: (1) development of green and environmentally friendly synthetic methods to reduce the dependence on transition metal catalysts, *e.g.*, synthesis of CMPs using light energy, or formation of desired CMPs by self-assembly of precursor molecules of CMPs. (2) Since nanomaterials such as nanowires, nanorods, nanotubes, and nanofibres have the characteristics of flexible materials, these materials are further combined with CMPs to develop flexible electrodes with good mechanical and electrochemical properties. (3) Integration of CMPs with flexible materials such as MXenes, carbon materials, and layered metal oxides is anticipated to augment the redox activity, theoretical capacity, and conductivity of electrode materials. (4) CMPs feature a highly crosslinked polymer network. Incorporating hyperbranching and alkylation techniques into the construction of CMP polymer networks, particularly on the linker and core, can enhance compatibility with the electrolyte and facilitate electrolyte penetration. This refinement promotes optimal activation of the active substances within the electrode. (5) Introduction of conjugated microporous polymer precursor molecules with flexible alkyl chains into the molecular design of CMPs can increase the flexibility of the precursor molecules. (6) In the design and synthesis of conjugated microporous polymers, precursor molecules such as quinoxaline-based aromatic heterocycles, aryl quinones and ketones, polyimides, and benzothiazoles should be included as much as possible to improve their electron transfer efficiency. (7) In order to improve the chemical and physical stability of CMPs, the degree of cross-linking of CMPs can be increased by introducing more stable chemical groups (sulfone, aryl groups, *etc.*) through chemical modification, which can make CMPs more reliable under extreme conditions (strong acids, bases, high temperatures, *etc.*).

In conclusion, although there are still some pressing issues regarding the synthesis methods and applications of CMPs, this does not detract from the fact that CMPs are an interesting "Möbius ring" with unlimited technological possibilities. We look forward to a bright future for CMP materials in various industrial applications.

Author contributions

D. Zhou and K. Q. Zhang co-authored the paper for this review. S. Q. Zou collected papers related to the topic of this review. X. B. Li and H. W. Ma: project administration, supervision, funding acquisition, writing. The paper was revised by all authors.

Conflicts of interest

There are no conflicts to declare.

Acknowledgements

This work was financially supported by the National Natural Science Foundation of China (22374017 and 62205052) and Fundamental Research Funds for the Central Universities (2572023CT12).

Notes and references

1 H. Cha, J. Kim, Y. Lee, J. Cho and M. Park, *Small*, 2017, **14**, 1702989.

2 T. M. Gür, *Energy Environ. Sci.*, 2018, **11**, 2696–2767.

3 S. Tao, R. Momen, Z. Luo, Y. Zhu, X. Xiao, Z. Cao, D. Xiong, W. Deng, Y. Liu, H. Hou, G. Zou and X. Ji, *Small*, 2023, **19**, 2207975.

4 M. Armand and J. M. Tarascon, *Nature*, 2008, **451**, 652–657.

5 J. Wang, Z. Wang, J. Ni and L. Li, *Energy Storage Mater.*, 2022, **45**, 704–719.

6 M. G. Mohamed, M. H. Elsayed, C. J. Li, A. E. Hassan, I. M. A. Mekhemer, A. F. Musa, M. K. Hussien, L. C. Chen, K. H. Chen, H. H. Chou and S. W. Kuo, *J. Mater. Chem. A*, 2024, **12**, 7693–7710.

7 Y. Zhao and J. Guo, *InfoMat*, 2020, **2**, 866–878.

8 P. N. Singh, M. G. Mohamed and S. W. Kuo, *ACS Appl. Energy Mater.*, 2023, **6**, 11342–11351.

9 Y. H. Zhu, X. Y. Yang, T. Liu and X. B. Zhang, *Adv. Mater.*, 2019, **32**, 1901961.

10 H. Cha, Y. Lee, J. Kim, M. Park and J. Cho, *Adv. Energy Mater.*, 2018, **8**, 1801917.

11 Z. Fang, J. Wang, H. Wu, Q. Li, S. Fan and J. Wang, *J. Power Sources*, 2020, **454**, 227932.

12 S. B. Huang, Y. Y. Hsieh, K. T. Chen and H. Y. Tuan, *Chem. Eng. J.*, 2021, **416**, 127697.

13 T. B. Schon, B. T. McAllister, P. F. Li and D. S. Seferos, *Chem. Soc. Rev.*, 2016, **45**, 6405–6406.

14 T. Yokoji, H. Matsubara and M. Satoh, *J. Mater. Chem. A*, 2014, **2**, 19347–19354.

15 C. Su, H. He, L. Xu, K. Zhao, C. Zheng and C. Zhang, *J. Mater. Chem. A*, 2017, **5**, 2701–2709.

16 C. Zhang, X. Yang, W. Ren, Y. Wang, F. Su and J. X. Jiang, *J. Power Sources*, 2016, **317**, 49–56.

17 S. Luo, Z. Zeng, H. Wang, W. Xiong, B. Song, C. Zhou, A. Duan, X. Tan, Q. He, G. Zeng, Z. Liu and R. Xiao, *Prog. Polym. Sci.*, 2021, **115**, 101374.

18 M. G. Mohamed, S. V. Chaganti, M. S. Li, M. M. Samy, S. U. Sharma, J. T. Lee, M. H. Elsayed, H. H. Chou and S. W. Kuo, *ACS Appl. Energy Mater.*, 2022, **5**, 6442–6452.

19 Y. Xu, S. Jin, H. Xu, A. Nagai and D. Jiang, *Chem. Soc. Rev.*, 2013, **42**, 8012–8031.

20 J. Chen, W. Yan, E. J. Townsend, J. Feng, L. Pan, V. Del Angel Hernandez and C. F. J. Faul, *Angew. Chem., Int. Ed.*, 2019, **58**, 11715–11719.

21 J. Chen, T. Qiu, W. Yan and C. F. J. Faul, *J. Mater. Chem. A*, 2020, **8**, 22657–22665.

22 K. Amin, N. Ashraf, L. Mao, C. F. J. Faul and Z. Wei, *Nano Energy*, 2021, **85**, 105958.

23 Z. Liu, Y. Yin, F. Xiu, X. Wang, S. Ju, M. Song, Q. Chang, J. Chen, J. Liu and W. Huang, *J. Mater. Chem. C*, 2018, **6**, 7295–7301.

24 H. T. Le, C. G. Wang and A. Goto, *Nat. Commun.*, 2023, **14**, 171.

25 T. H. Weng, M. G. Mohamed, S. U. Sharma, I. M. A. Mekhemer, H. H. Chou and S. W. Kuo, *ACS Appl. Energy Mater.*, 2023, **6**, 9012–9024.

26 H. Liu, Y. Wang, W. Mo, H. Tang, Z. Cheng, Y. Chen, S. Zhang, H. Ma, B. Li and X. Li, *Adv. Funct. Mater.*, 2020, **30**, 1910275.
27 Z. Q. Chen, T. Chen, J. X. Liu, G. F. Zhang, C. Li, W. L. Gong, Z. J. Xiong, N. H. Xie, B. Z. Tang and M. Q. Zhu, *Macromolecules*, 2015, **48**, 7823–7835.
28 M. Liu, B. Zhou, L. Zhou, Z. Xie, S. Li and L. Chen, *J. Mater. Chem. A*, 2018, **6**, 9860–9865.
29 Y. Zang, S. Gao, B. Jing, H. Sun, J. Wang, J. Liu, F. Miao and L. Xu, *J. Mater. Sci.*, 2022, **58**, 170–185.
30 X. Cheng, R. Guan, Z. Wu, Y. Sun, W. Che and Q. Shang, *InfoMat*, 2024, e12535, DOI: 10.1002/inf2.12535.
31 C. J. Sun, X. Q. Zhao, P. F. Wang, H. Wang and B. H. Han, *Sci. China: Chem.*, 2017, **60**, 1067–1074.
32 M. G. Mohamed, W. C. Chang, S. V. Chaganti, S. U. Sharma, J. T. Lee and S. W. Kuo, *Polym. Chem.*, 2023, **14**, 4589–4601.
33 I. Ullah, T. A. Taha, A. M. Alenad, I. Uddin, A. Hayat, A. Hayat, M. Sohail, A. Irfan, J. Khan and A. Palamanit, *Surf. Interfaces*, 2021, **25**, 101227.
34 Q. Zhang, S. Yu, Q. Wang, Q. Xiao, Y. Yue and S. Ren, *Macromol. Rapid Commun.*, 2017, **38**, 1700445.
35 C. Hu, Y. C. Gao, C. Zhang, M. Liu and T. M. Geng, *RSC Adv.*, 2020, **10**, 5108–5115.
36 I. M. A. Mekhemer, M. M. Elsenety, A. M. Elewa, K. D. G. Huynh, M. M. Samy, M. G. Mohamed, D. M. Dorrah, D. C. K. Hoang, A. F. Musa, S. W. Kuo and H. H. Chou, *J. Mater. Chem. A*, 2024, **12**, 10790–10798.
37 C. W. Kang, Y. J. Ko and H. Jin Kim, *J. Mater. Chem. A*, 2021, **9**, 17978–17984.
38 P. N. Singh, M. G. Mohamed, S. V. Chaganti, S. U. Sharma, M. Ejaz, J. T. Lee and S. W. Kuo, *ACS Appl. Energy Mater.*, 2023, **6**, 8277–8287.
39 C. Gu, N. Huang, J. Gao, F. Xu, Y. Xu and D. Jiang, *Angew. Chem., Int. Ed.*, 2014, **53**, 4850–4855.
40 M. Ejaz, M. G. Mohamed, W. C. Huang and S. W. Kuo, *J. Mater. Chem. A*, 2023, **11**, 22868–22883.
41 K. Yuan, P. G. Wang, T. Hu, L. Shi, R. Zeng, M. Forster, T. Pichler, Y. Chen and U. Scherf, *Chem. Mater.*, 2015, **27**, 7403–7411.
42 J. M. Lee and A. I. Cooper, *Chem. Rev.*, 2020, **120**, 2171–2214.
43 F. S. J. X. Jiang, A. Trewin, C. D. Wood, H. J. Niu, J. T. A. Jones, Y. Z. Khimyak and A. I. Cooper, *J. Am. Chem. Soc.*, 2008, **130**, 7710–7720.
44 F. Xu, X. Chen, Z. Tang, D. Wu, R. Fu and D. Jiang, *Chem. Commun.*, 2014, **50**, 4788–4790.
45 M. G. Mohamed, S. V. Chaganti, S. U. Sharma, M. M. Samy, M. Ejaz, J. T. Lee, K. Zhang and S. W. Kuo, *ACS Appl. Energy Mater.*, 2022, **5**, 10130–10140.
46 N. Miyaura and A. Suzuki, *J. Chem. Soc., Chem. Commun.*, 1979, 866–867.
47 K. Y. Norio Miyaura and A. Suzuki, *Tetrahedron Lett.*, 1979, **36**, 3437–3440.
48 B. Bonillo, R. S. Sprick and A. I. Cooper, *Chem. Mater.*, 2016, **28**, 3469–3480.
49 C. Zhang, Y. Qiao, P. Xiong, W. Ma, P. Bai, X. Wang, Q. Li, J. Zhao, Y. Xu, Y. Chen, J. H. Zeng, F. Wang, Y. Xu and J. X. Jiang, *ACS Nano*, 2019, **13**, 745–754.
50 S. B. Ren, W. Ma, C. Zhang, L. Chen, K. Wang, R. R. Li, M. Shen, D. M. Han, Y. Chen and J. X. Jiang, *ChemSusChem*, 2020, **13**, 2295–2302.
51 M. G. Kotp, N. L. Torad, H. Nara, W. Chaikittisilp, J. You, Y. Yamauchi, A. F. M. El-Mahdy and S. W. Kuo, *J. Mater. Chem. A*, 2023, **11**, 15022–15032.
52 R. F. Heck, *J. Am. Chem. Soc.*, 1968, **90**, 5518–5526.
53 L. Sun, Z. Liang, J. Yu and R. Xu, *Polym. Chem.*, 2013, **4**, 1932–1938.
54 A. S. Guram and S. L. Buchwald, *J. Am. Chem. Soc.*, 1994, **116**, 7901–7902.
55 Y. Liao, J. Weber and C. F. J. Faul, *Chem. Commun.*, 2014, **50**, 8002–8005.
56 Y. Liao, J. Weber, B. M. Mills, Z. Ren and C. F. J. Faul, *Macromolecules*, 2016, **49**, 6322–6333.
57 L. Pan, Z. Liu, M. Tian, B. C. Schroeder, A. E. Aliev and C. F. J. Faul, *ACS Appl. Mater. Interfaces*, 2019, **11**, 48352–48362.
58 H. Y. Yamamoto Takakazu and Y. Akio, *Bull. Chem. Soc. Jpn.*, 1978, **51**, 2091–2097.
59 Z. H. Zhou and T. Yamamoto, *J. Organomet. Chem.*, 1991, **414**, 119–127.
60 J. R. Holst, E. Stöckel, D. J. Adams and A. I. Cooper, *Macromolecules*, 2010, **43**, 8531–8538.
61 J. Schmidt, M. Werner and A. Thomas, *Macromolecules*, 2009, **42**, 4426–4429.
62 Z. Tan, H. Su, Y. Guo, H. Liu, B. Liao, A. M. Amin and Q. Liu, *Polymers*, 2020, **12**(3), 719.
63 Q. He, J. Kang, J. Zhu, S. Huang, C. Lu, H. Liang, Y. Su and X. Zhuang, *Chem. Commun.*, 2022, **58**, 2339–2342.
64 M. Grzybowski, K. Skonieczny, H. Butenschön and D. T. Gryko, *Angew. Chem., Int. Ed.*, 2013, **52**, 9900–9930.
65 T. A. Mitsuru Ueda and H. Awano, *Macromolecules*, 1992, **25**, 5125–5130.
66 Q. Chen, D. P. Liu, M. Luo, L. J. Feng, Y. C. Zhao and B. H. Han, *Small*, 2014, **10**, 308–315.
67 W. Wei, G. Chang, Y. Xu and L. Yang, *J. Mater. Chem. A*, 2018, **6**, 18794–18798.
68 L. Lian, K. Li, L. Ren, D. Han, X. Lv and H. G. Wang, *Colloids Surf., A*, 2023, **657**, 130496.
69 W. Hao, R. Chen, Y. Zhang, Y. Wang and Y. Zhao, *ACS Omega*, 2021, **6**, 23782–23787.
70 M. Mohamed Samy, I. M. A. Mekhemer, M. G. Mohamed, M. Hammad Elsayed, K. H. Lin, Y. K. Chen, T. L. Wu, H. H. Chou and S. W. Kuo, *Chem. Eng. J.*, 2022, **446**, 137158.
71 J. W. F. Y. Meng, M. H. Chen, Z. G. Wang, G. Y. Bai and X. W. Lan, *ACS Catal.*, 2023, **13**, 12142–12152.
72 Y. Kou, Y. Xu, Z. Guo and D. Jiang, *Angew. Chem., Int. Ed.*, 2011, **50**, 8753–8757.
73 O. Buyukcakir, R. Yuksel, Y. Jiang, S. H. Lee, W. K. Seong, X. Chen and R. S. Ruoff, *Angew. Chem., Int. Ed.*, 2018, **58**, 872–876.
74 J. Kim, M. H. Le, M. C. Spicer, C. M. Moisanu, S. M. Pugh and P. J. Milner, *J. Mater. Chem. A*, 2023, **11**, 17159–17166.
75 S. Y. Yu, J. Mahmood, H. J. Noh, J. M. Seo, S. M. Jung, S. H. Shin, Y. K. Im, I. Y. Jeon and J. B. Baek, *Angew. Chem., Int. Ed.*, 2018, **57**, 8438–8442.

76 Y. Zhu, X. Chen, Y. Cao, W. Peng, Y. Li, G. Zhang, F. Zhang and X. Fan, *Chem. Commun.*, 2019, **55**, 1434–1437.
77 E. T. Seo, J. M. Fritsch, L. S. Marcoux, D. W. Leedy and R. N. Adams, *J. Am. Chem. Soc.*, 1966, **88**, 3498–3503.
78 R. F. Nelson and J. F. Ambrose, *J. Electrochem. Soc.*, 1968, **115**, 1159–1164.
79 H. Ma, Y. Chen, X. Li and B. Li, *Adv. Funct. Mater.*, 2021, **31**, 2101861.
80 H. Ma, F. Li, P. Li, H. Wang, M. Zhang, G. Zhang, M. Baumgarten and K. Müllen, *Adv. Funct. Mater.*, 2016, **26**, 2025–2031.
81 W. Mo, Z. Zhu, F. Kong, X. Li, Y. Chen, H. Liu, Z. Cheng, H. Ma and B. Li, *Nat. Commun.*, 2022, **13**, 5189.
82 A. Hayat, M. Sohail, A. El Jery, K. M. Al-Zaydi, S. Raza, H. Ali, Y. Al-Hadeethi, T. A. Taha, I. Ud Din, M. Ali Khan, M. A. Amin, E. Ghasali, Y. Orooji, Z. Ajmal and M. Zahid Ansari, *Mater. Today*, 2023, **64**, 180–208.
83 K. Y. Lin and A. F. M. El-Mahdy, *Mater. Chem. Phys.*, 2022, **281**, 125850.
84 J. Kim, C. M. Moisanu, C. N. Gannett, A. Halder, J. J. Fuentes-Rivera, S. H. Majer, K. M. Lancaster, A. C. Forse, H. D. Abruña and P. J. Milner, *Chem. Mater.*, 2021, **33**, 8334–8342.
85 E. Troschke, S. Grätz, T. Lübken and L. Borchardt, *Angew. Chem., Int. Ed.*, 2017, **56**, 6859–6863.
86 Y. Q. Hu, C. Zhou, X. Huang, B. An, R. Wang, F. Lan and X. Zhang, *ACS Sustainable Chem. Eng.*, 2023, **11**, 10225–10232.
87 B. Tian, J. Zheng, C. Zhao, C. Liu, C. Su, W. Tang, X. Li and G. H. Ning, *J. Mater. Chem. A*, 2019, **7**, 9997–10003.
88 L. Shu, J. Yu, Y. Cui, Y. Ma, Y. Li, B. Gao and H. G. Wang, *Int. J. Hydrogen Energy*, 2022, **47**, 10902–10910.
89 F. Cheng and J. Chen, *Chem. Soc. Rev.*, 2012, **41**, 1111–1129.
90 Y. G. Li and J. Lu, *ACS Energy Lett.*, 2017, **2**, 1370–1377.
91 Y. Liang, Z. Tao and J. Chen, *Adv. Energy Mater.*, 2012, **2**, 742–769.
92 C. Luo, X. Ji, S. Hou, N. Eidson, X. Fan, Y. Liang, T. Deng, J. Jiang and C. Wang, *Adv. Mater.*, 2018, **30**, 1706498.
93 J. Wang, C. S. Chen and Y. Zhang, *ACS Sustain. Chem. Eng.*, 2017, **6**, 1772–1779.
94 D. J. Kim, D. J. Yoo, M. T. Otley, A. Prokofjevs, C. Pezzato, M. Owczarek, S. J. Lee, J. W. Choi and J. F. Stoddart, *Nat. Energy*, 2018, **4**, 51–59.
95 C. Peng, G. H. Ning, J. Su, G. Zhong, W. Tang, B. Tian, C. Su, D. Yu, L. Zu, J. Yang, M. F. Ng, Y. S. Hu, Y. Yang, M. Armand and K. P. Loh, *Nat. Energy*, 2017, **2**, 17074.
96 S. Zhang, W. Huang, P. Hu, C. Huang, C. Shang, C. Zhang, R. Yang and G. Cui, *J. Mater. Chem. A*, 2015, **3**, 1896–1901.
97 S. Xu, G. Wang, B. P. Biswal, M. Addicoat, S. Paasch, W. Sheng, X. Zhuang, E. Brunner, T. Heine, R. Berger and X. Feng, *Angew. Chem., Int. Ed.*, 2018, **58**, 849–853.
98 W. Ma, C. Zhang, X. Gao, C. Shu, C. Yan, F. Wang, Y. Chen, J. H. Zeng and J. X. Jiang, *J. Power Sources*, 2020, **453**, 227868.
99 C. Zhang, Y. He, P. Mu, X. Wang, Q. He, Y. Chen, J. Zeng, F. Wang, Y. Xu and J. X. Jiang, *Adv. Funct. Mater.*, 2018, **28**, 1705432.
100 L. Zhong, Z. Fang, C. Shu, C. Mo, X. Chen and D. Yu, *Angew. Chem., Int. Ed.*, 2021, **60**, 10164–10171.
101 J. Min Park, J. H. Lee and W. D. Jang, *Coord. Chem. Rev.*, 2020, **407**, 213157.
102 P. Gao, Z. Chen, Z. Zhao Karger, J. E. Mueller, C. Jung, S. Klyatskaya, T. Diemant, O. Fuhr, T. Jacob, R. J. Behm, M. Ruben and M. Fichtner, *Angew. Chem., Int. Ed.*, 2017, **56**, 10341–10346.
103 Y. Yang, J. Yuan, S. Huang, Z. Chen, C. Lu, C. Yang, G. Zhai, J. Zhu and X. Zhuang, *J. Power Sources*, 2022, **531**, 231340.
104 A. Molina, N. Patil, E. Ventosa, M. Liras, J. Palma and R. Marcilla, *Adv. Funct. Mater.*, 2019, **30**, 1908074.
105 R. Grieco, A. Molina, J. S. Sanchez, N. Patil, M. Liras and R. Marcilla, *Mater. Today Energy*, 2022, **27**, 101014.
106 H. Zhang, L. Zhong, J. Xie, F. Yang, X. Liu and X. Lu, *Adv. Mater.*, 2021, **33**, 2101857.
107 R. Grieco, O. Luzanin, D. Alván, M. Liras, R. Dominko, N. Patil, J. Bitenc and R. Marcilla, *Faraday Discuss.*, 2024, **250**, 110–128.
108 G. Dai, Y. He, Z. Niu, P. He, C. Zhang, Y. Zhao, X. Zhang and H. Zhou, *Angew. Chem., Int. Ed.*, 2019, **58**, 9902–9906.
109 C. N. Gannett, B. M. Peterson, L. Melecio-Zambrano, C. Q. Trainor, B. P. Fors and H. D. Abruña, *J. Mater. Chem. A*, 2021, **9**, 5657–5663.
110 G. Dai, Y. Liu, Z. Niu, P. He, Y. Zhao, X. Zhang and H. Zhou, *Matter*, 2019, **1**, 945–958.
111 W. Ma, L. W. Luo, X. Huang, P. Dong, Y. Chen, C. Zhang, F. Huang, J. X. Jiang and Y. Cao, *Adv. Energy Mater.*, 2022, **13**, 2203253.
112 W. Ma, L. W. Luo, P. Dong, P. Zheng, X. Huang, C. Zhang, J. X. Jiang and Y. Cao, *Adv. Funct. Mater.*, 2021, **31**, 2105027.
113 R. Liu, C. Wei, X. Liu, Y. Qu, L. Yan, H. Zhao, Y. Wu, H. Cao, J. Li and H. Wang, *J. Mater. Sci.: Mater. Electron.*, 2023, **34**, 159.
114 Z. Ouyang, D. Tranca, Y. Zhao, Z. Chen, X. Fu, J. Zhu, G. Zhai, C. Ke, E. Kymakis and X. Zhuang, *ACS Appl. Mater. Interfaces*, 2021, **13**, 9064–9073.
115 S. Liu, L. Kang, J. Zhang, E. Jung, S. Lee and S. C. Jun, *Energy Storage Mater.*, 2020, **32**, 167–177.
116 Z. Xu, S. Sun, Y. Han, Z. Wei, Y. Cheng, S. Yin and W. Cui, *ACS Appl. Energy Mater.*, 2020, **3**, 5393–5404.
117 M. Ahmed, M. G. Kotp, T. H. Mansoure, R. H. Lee, S. W. Kuo and A. F. M. El-Mahdy, *Microporous Mesoporous Mater.*, 2022, **333**, 111766.
118 J. Kim, J. H. Kim and K. Ariga, *Joule*, 2017, **1**, 739–768.
119 H. Zhao, J. Wang, Y. Zheng, J. Li, X. Han, G. He and Y. Du, *Angew. Chem., Int. Ed.*, 2017, **56**, 15334–15338.
120 Y. Wang, W. Li, L. Zhang, X. Zhang, B. Tan, J. Hao, Z. Jian, X. Wang, Q. Hu and X. Lu, *J. Power Sources*, 2020, **449**, 227487.
121 M. G. Mohamed, C. C. Lee, A. F. M. El-Mahdy, J. Lüder, M.-H. Yu, Z. Li, Z. Zhu, C. C. Chueh and S.-W. Kuo, *J. Mater. Chem. A*, 2020, **8**, 11448–11459.
122 D. Kim, J. Kang, B. Yan, K. d. Seong and Y. Piao, *ACS Sustain. Chem. Eng.*, 2020, **8**, 2843–2853.
123 M. G. Mohamed, M. M. Samy, T. H. Mansoure, S. U. Sharma, M. S. Tsai, J. H. Chen, J. T. Lee and S. W. Kuo, *ACS Appl. Energy Mater.*, 2022, **5**, 3677–3688.

124 X. C. Li, Y. Zhang, C. Y. Wang, Y. Wan, W. Y. Lai, H. Pang and W. Huang, *Chem. Sci.*, 2017, **8**, 2959–2965.

125 X. Liu, G. Sun, Y. Gong, C. F. Liu, S. Wang, S. Xu, X. Yang, L. Yang and W. Y. Lai, *Sci. China: Chem.*, 2022, **65**, 1767–1774.

126 Y. Liao, H. Wang, M. Zhu and A. Thomas, *Adv. Mater.*, 2018, **30**, 1705710.

127 D. P. Dubal, N. R. Chodankar, D. H. Kim and P. Gomez-Romero, *Chem. Soc. Rev.*, 2018, **47**, 2065–2129.

128 L. Wang, X. Fu, J. He, X. Shi, T. Chen, P. Chen, B. Wang and H. Peng, *Adv. Mater.*, 2019, **32**, 1901971.

129 Y. Li, X. Yan, X. Zheng, H. Si, M. Li, Y. Liu, Y. Sun, Y. Jiang and Y. Zhang, *J. Mater. Chem. A*, 2016, **4**, 17704–17710.

130 Z. Pan, J. Yang, Q. Zhang, M. Liu, Y. Hu, Z. Kou, N. Liu, X. Yang, X. Ding, H. Chen, J. Li, K. Zhang, Y. Qiu, Q. Li, J. Wang and Y. Zhang, *Adv. Energy Mater.*, 2019, **9**, 1802753.

131 W. Lyu, W. Zhang, H. Liu, Y. Liu, H. Zuo, C. Yan, C. F. J. Faul, A. Thomas, M. Zhu and Y. Liao, *Chem. Mater.*, 2020, **32**, 8276–8285.

132 M. Khalid and H. Varela, *J. Mater. Chem. A*, 2018, **6**, 3141–3150.

133 J. Cao, Y. Zhao, Y. Xu, Y. Zhang, B. Zhang and H. Peng, *J. Mater. Chem. A*, 2018, **6**, 3355–3360.

134 X. Zhuang, F. Zhang, D. Wu and X. Feng, *Adv. Mater.*, 2014, **26**, 3081–3086.

135 Z. S. Wu, Y. Zheng, S. Zheng, S. Wang, C. Sun, K. Parvez, T. Ikeda, X. Bao, K. Müllen and X. Feng, *Adv. Mater.*, 2016, **29**, 1602960.

136 L. Mei, X. Cui, J. Wei, Q. Duan and Y. Li, *Dyes Pigm.*, 2021, **190**, 109299.

137 R. K. Pavel, A. Troshin, A. S. Peregudov, S. M. Peregudova, M. Egginger, R. N. Lyubovskaya and N. Serdar Sariciftci, *Chem. Mater.*, 2007, **19**, 5363–5372.

138 J. Mu, C. Shao, Z. Guo, M. Zhang, Z. Zhang, P. Zhang, B. Chen and Y. Liu, *Nanoscale*, 2011, **3**, 5126–5131.

139 Z. Cabrane, M. Ouassaid and M. Maaroufi, *Int. J. Hydrogen Energy*, 2016, **41**, 20897–20907.

140 H. Ahn, Y. C. Huang, C. W. Lin, Y. L. Chiu, E. C. Lin, Y. Y. Lai and Y. H. Lee, *ACS Appl. Mater. Interfaces*, 2018, **10**, 29145–29152.

141 K. I. O. Alfred and T. Chidembo, *Electroanalysis*, 2010, **22**, 2529–2535.

142 X. C. Lan Mei, Q. Duan, Y. Li, X. Lv and H. Wang, *Int. J. Hydrogen Energy*, 2020, **45**, 22950–22958.

143 A. Modak, M. Nandi, J. Mondal and A. Bhaumik, *Chem. Commun.*, 2012, **48**, 248–250.

144 E. L. Spitler, J. W. Colson, F. J. Uribe-Romo, A. R. Woll, M. R. Giovino, A. Saldivar and W. R. Dichtel, *Angew. Chem., Int. Ed.*, 2012, **51**, 2623–2627.

145 L. Mei, J. C. Wei and Q. Duan, *J. Mater. Sci.: Mater. Electron.*, 2021, **32**, 24953–24963.

146 T. A. Gaber, L. R. Ahmed and A. F. M. El-Mahdy, *J. Mater. Chem. A*, 2023, **11**, 19408–19417.

147 M. Jang, Y. Cho, Y. Kim, M. Hahn, D. Jung, S. Y. Park, W. Lee and Y. Piao, *Electrochim. Acta*, 2022, **434**, 141315.

148 C. D. X. Wang, S.-H. Lee, K. J. Senecal, J. Kumar and L. A. Samuelson, *Nano Lett.*, 2002, **2**, 1273–1275.

149 Y. Wang, A. La, Y. Ding, Y. Liu and Y. Lei, *Adv. Funct. Mater.*, 2012, **22**, 3547–3555.

150 R. M. DuChanois, C. J. Porter, C. Violet, R. Verduzco and M. Elimelech, *Adv. Mater.*, 2021, **33**, 2101312.

151 Z. Zhou, D. B. Shinde, D. Guo, L. Cao, R. A. Nuaimi, Y. Zhang, L. R. Enakonda and Z. Lai, *Adv. Funct. Mater.*, 2021, **32**, 2108672.

152 F. Ren, F. Wang, Y. Pan, H. Sun, Z. Zhu, C. Ma, C. Xiao, W. Liang, L. Chen and A. Li, *Macromol. Mater. Eng.*, 2018, **303**, 1700619.

153 B. Prusti, S. Tripathi, P. K. Samanta and M. Chakravarty, *Adv. Opt. Mater.*, 2024, **12**, 2301746.

154 Z. Li, W. Wang, Y. Xu, Y. Zhu and X. Guo, *J. CO_2 Util.*, 2021, **49**, 101550.